Amplitude analysis of the $\pi^0\pi^0$ system produced in radiative J/ψ decays

M. Ablikim,[1] M. N. Achasov,[9,f] X. C. Ai,[1] O. Albayrak,[5] M. Albrecht,[4] D. J. Ambrose,[44] A. Amoroso,[48a,48c] F. F. An,[1] Q. An,[45,a] J. Z. Bai,[1] R. Baldini Ferroli,[20a] Y. Ban,[31] D. W. Bennett,[19] J. V. Bennett,[5] M. Bertani,[20a] D. Bettoni,[21a] J. M. Bian,[43] F. Bianchi,[48a,48c] E. Boger,[23,d] O. Bondarenko,[25] I. Boyko,[23] R. A. Briere,[5] H. Cai,[50] X. Cai,[1,a] O. Cakir,[40a,b] A. Calcaterra,[20a] G. F. Cao,[1] S. A. Cetin,[40b] J. F. Chang,[1,a] G. Chelkov,[23,d,e] G. Chen,[1] H. S. Chen,[1] H. Y. Chen,[2] J. C. Chen,[1] M. L. Chen,[1,a] S. J. Chen,[29] X. Chen,[1,a] X. R. Chen,[26] Y. B. Chen,[1,a] H. P. Cheng,[17] X. K. Chu,[31] G. Cibinetto,[21a] D. Cronin-Hennessy,[43] H. L. Dai,[1,a] J. P. Dai,[34] A. Dbeyssi,[14] D. Dedovich,[23] Z. Y. Deng,[1] A. Denig,[22] I. Denysenko,[23] M. Destefanis,[48a,48c] F. De Mori,[48a,48c] Y. Ding,[27] C. Dong,[30] J. Dong,[1,a] L. Y. Dong,[1] M. Y. Dong,[1,a] S. X. Du,[52] P. F. Duan,[1] E. E. Eren,[40b] J. Z. Fan,[39] J. Fang,[1,a] S. S. Fang,[1] X. Fang,[45,a] Y. Fang,[1] L. Fava,[48b,48c] F. Feldbauer,[22] G. Felici,[20a] C. Q. Feng,[45,a] E. Fioravanti,[21a] M. Fritsch,[14,22] C. D. Fu,[1] Q. Gao,[1] X. Y. Gao,[2] Y. Gao,[39] Z. Gao,[45,a] I. Garzia,[21a] C. Geng,[45,a] K. Goetzen,[10] W. X. Gong,[1,a] W. Gradl,[22] M. Greco,[48a,48c] M. H. Gu,[1,a] Y. T. Gu,[12] Y. H. Guan,[1] A. Q. Guo,[1] L. B. Guo,[28] Y. Guo,[1] Y. P. Guo,[22] Z. Haddadi,[25] A. Hafner,[22] S. Han,[50] Y. L. Han,[1] X. Q. Hao,[15] F. A. Harris,[42] K. L. He,[1] Z. Y. He,[30] T. Held,[4] Y. K. Heng,[1,a] Z. L. Hou,[1] C. Hu,[28] H. M. Hu,[1] J. F. Hu,[48a,48c] T. Hu,[1,a] Y. Hu,[1] G. M. Huang,[6] G. S. Huang,[45,a] H. P. Huang,[50] J. S. Huang,[15] X. T. Huang,[33] Y. Huang,[29] T. Hussain,[47] Q. Ji,[1] Q. P. Ji,[30] X. B. Ji,[1] X. L. Ji,[1,a] L. L. Jiang,[1] L. W. Jiang,[50] X. S. Jiang,[1,a] X. Y. Jiang,[30] J. B. Jiao,[33] Z. Jiao,[17] D. P. Jin,[1,a] S. Jin,[1] T. Johansson,[49] A. Julin,[43] N. Kalantar-Nayestanaki,[25] X. L. Kang,[1] X. S. Kang,[30] M. Kavatsyuk,[25] B. C. Ke,[5] P. Kiese,[22] R. Kliemt,[14] B. Kloss,[22] O. B. Kolcu,[40b,i] B. Kopf,[4] M. Kornicer,[42] W. Kühn,[24] A. Kupsc,[49] J. S. Lange,[24] M. Lara,[19] P. Larin,[14] C. Leng,[48c] C. Li,[49] C. H. Li,[1] Cheng Li,[45,a] D. M. Li,[52] F. Li,[1,a] G. Li,[1] H. B. Li,[1] J. C. Li,[1] Jin Li,[32] K. Li,[13] K. Li,[33] Lei Li,[3] P. R. Li,[41] T. Li,[33] W. D. Li,[1] W. G. Li,[1] X. L. Li,[33] X. M. Li,[12] X. N. Li,[1,a] X. Q. Li,[30] Z. B. Li,[38] H. Liang,[45,a] Y. F. Liang,[36] Y. T. Liang,[24] G. R. Liao,[11] D. X. Lin,[14] B. J. Liu,[1] C. X. Liu,[1] F. H. Liu,[35] Fang Liu,[1] Feng Liu,[6] H. B. Liu,[12] H. H. Liu,[16] H. H. Liu,[1] H. M. Liu,[1] J. Liu,[1] J. B. Liu,[45,a] J. P. Liu,[50] J. Y. Liu,[1] K. Liu,[39] K. Y. Liu,[27] L. D. Liu,[31] P. L. Liu,[1,a] Q. Liu,[41] S. B. Liu,[45,a] X. Liu,[26] X. X. Liu,[41] Y. B. Liu,[30] Z. A. Liu,[1,a] Zhiqiang Liu,[1] Zhiqing Liu,[22] H. Loehner,[25] X. C. Lou,[1,a,h] H. J. Lu,[17] J. G. Lu,[1,a] R. Q. Lu,[18] Y. Lu,[1] Y. P. Lu,[1,a] C. L. Luo,[28] M. X. Luo,[51] T. Luo,[42] X. L. Luo,[1,a] M. Lv,[1] X. R. Lyu,[41] F. C. Ma,[27] H. L. Ma,[1] L. L. Ma,[33] Q. M. Ma,[1] T. Ma,[1] X. N. Ma,[30] X. Y. Ma,[1,a] F. E. Maas,[14] M. Maggiora,[48a,48c] Q. A. Malik,[47] Y. J. Mao,[31] Z. P. Mao,[1] S. Marcello,[48a,48c] J. G. Messchendorp,[25] J. Min,[1,a] T. J. Min,[1] R. E. Mitchell,[19] X. H. Mo,[1,a] Y. J. Mo,[6] C. Morales Morales,[14] K. Moriya,[19] N. Yu. Muchnoi,[9,f] H. Muramatsu,[43] Y. Nefedov,[23] F. Nerling,[14] I. B. Nikolaev,[9,f] Z. Ning,[1,a] S. Nisar,[8] S. L. Niu,[1,a] X. Y. Niu,[1] S. L. Olsen,[32] Q. Ouyang,[1,a] S. Pacetti,[20b] P. Patteri,[20a] M. Pelizaeus,[4] H. P. Peng,[45,a] K. Peters,[10] J. Pettersson,[49] J. L. Ping,[28] R. G. Ping,[1] R. Poling,[43] V. Prasad,[1] Y. N. Pu,[18] M. Qi,[29] S. Qian,[1,a] C. F. Qiao,[41] L. Q. Qin,[33] N. Qin,[50] X. S. Qin,[1] Y. Qin,[31] Z. H. Qin,[1,a] J. F. Qiu,[1] K. H. Rashid,[47] C. F. Redmer,[22] H. L. Ren,[18] M. Ripka,[22] G. Rong,[1] Ch. Rosner,[14] X. D. Ruan,[12] V. Santoro,[21a] A. Sarantsev,[23,g] M. Savrié,[21b] K. Schoenning,[49] S. Schumann,[22] W. Shan,[31] M. Shao,[45,a] C. P. Shen,[2] P. X. Shen,[30] X. Y. Shen,[1] H. Y. Sheng,[1] M. R. Shepherd,[19] W. M. Song,[1] X. Y. Song,[1] S. Sosio,[48a,48c] S. Spataro,[48a,48c] G. X. Sun,[1] J. F. Sun,[15] S. S. Sun,[1] Y. J. Sun,[45,a] Y. Z. Sun,[1] Z. J. Sun,[1,a] Z. T. Sun,[19] C. J. Tang,[36] X. Tang,[1] I. Tapan,[40c] E. H. Thorndike,[44] M. Tiemens,[25] D. Toth,[43] M. Ullrich,[24] I. Uman,[40b] G. S. Varner,[42] B. Wang,[30] B. L. Wang,[41] D. Wang,[31] D. Y. Wang,[31] K. Wang,[1,a] L. L. Wang,[1] L. S. Wang,[1] M. Wang,[33] P. Wang,[1] P. L. Wang,[1] S. G. Wang,[31] W. Wang,[1,a] X. F. Wang,[39] Y. D. Wang,[14] Y. F. Wang,[1,a] Y. Q. Wang,[22] Z. Wang,[1,a] Z. G. Wang,[1,a] Z. H. Wang,[45,a] Z. Y. Wang,[1] T. Weber,[22] D. H. Wei,[11] J. B. Wei,[31] P. Weidenkaff,[22] S. P. Wen,[1] U. Wiedner,[4] M. Wolke,[49] L. H. Wu,[1] Z. Wu,[1,a] L. G. Xia,[39] Y. Xia,[18] D. Xiao,[1] Z. J. Xiao,[28] Y. G. Xie,[1,a] Q. L. Xiu,[1,a] G. F. Xu,[1] L. Xu,[1] Q. J. Xu,[13] Q. N. Xu,[41] X. P. Xu,[37] L. Yan,[45,a] W. B. Yan,[45,a] W. C. Yan,[45,a] Y. H. Yan,[18] H. X. Yang,[1] L. Yang,[50] Y. Yang,[6] Y. X. Yang,[11] H. Ye,[1] M. Ye,[1,a] M. H. Ye,[7] J. H. Yin,[1] B. X. Yu,[1,a] C. X. Yu,[30] H. W. Yu,[31] J. S. Yu,[26] C. Z. Yuan,[1] W. L. Yuan,[29] Y. Yuan,[1] A. Yuncu,[40b,c] A. A. Zafar,[47] A. Zallo,[20a] Y. Zeng,[18] B. X. Zhang,[1] B. Y. Zhang,[1,a] C. Zhang,[29] C. C. Zhang,[1] D. H. Zhang,[1] H. H. Zhang,[38] H. Y. Zhang,[1,a] J. J. Zhang,[1] J. L. Zhang,[1] J. Q. Zhang,[1] J. W. Zhang,[1,a] J. Y. Zhang,[1] J. Z. Zhang,[1] K. Zhang,[1] L. Zhang,[1] S. H. Zhang,[1] X. Y. Zhang,[33] Y. Zhang,[1] Y. N. Zhang,[41] Y. H. Zhang,[1,a] Y. T. Zhang,[45,a] Yu Zhang,[41] Z. H. Zhang,[6] Z. P. Zhang,[45] Z. Y. Zhang,[50] G. Zhao,[1] J. W. Zhao,[1,a] J. Y. Zhao,[1] J. Z. Zhao,[1,a] Lei Zhao,[45,a] Ling Zhao,[1] M. G. Zhao,[30] Q. Zhao,[1] Q. W. Zhao,[1] S. J. Zhao,[52] T. C. Zhao,[1] Y. B. Zhao,[1,a] Z. G. Zhao,[45,a] A. Zhemchugov,[23,d] B. Zheng,[46] J. P. Zheng,[1,a] W. J. Zheng,[33] Y. H. Zheng,[41] B. Zhong,[28] L. Zhou,[1,a] Li Zhou,[30] X. Zhou,[50] X. K. Zhou,[45,a] X. R. Zhou,[45,a] X. Y. Zhou,[1] K. Zhu,[1] K. J. Zhu,[1,a] S. Zhu,[1] X. L. Zhu,[39] Y. C. Zhu,[45,a] Y. S. Zhu,[1] Z. A. Zhu,[1] J. Zhuang,[1,a] L. Zotti,[48a,48c] B. S. Zou,[1] and J. H. Zou[1]

(BESIII Collaboration)

A. P. Szczepaniak,[19,53,54] and P. Guo[19,53]

[1]*Institute of High Energy Physics, Beijing 100049, People's Republic of China*
[2]*Beihang University, Beijing 100191, People's Republic of China*
[3]*Beijing Institute of Petrochemical Technology, Beijing 102617, People's Republic of China*
[4]*Bochum Ruhr-University, D-44780 Bochum, Germany*
[5]*Carnegie Mellon University, Pittsburgh, Pennsylvania 15213, USA*
[6]*Central China Normal University, Wuhan 430079, People's Republic of China*
[7]*China Center of Advanced Science and Technology, Beijing 100190, People's Republic of China*
[8]*COMSATS Institute of Information Technology, Lahore,
Defence Road, Off Raiwind Road, 54000 Lahore, Pakistan*
[9]*G. I. Budker Institute of Nuclear Physics SB RAS (BINP), Novosibirsk 630090, Russia*
[10]*GSI Helmholtzcentre for Heavy Ion Research GmbH, D-64291 Darmstadt, Germany*
[11]*Guangxi Normal University, Guilin 541004, People's Republic of China*
[12]*GuangXi University, Nanning 530004, People's Republic of China*
[13]*Hangzhou Normal University, Hangzhou 310036, People's Republic of China*
[14]*Helmholtz Institute Mainz, Johann-Joachim-Becher-Weg 45, D-55099 Mainz, Germany*
[15]*Henan Normal University, Xinxiang 453007, People's Republic of China*
[16]*Henan University of Science and Technology, Luoyang 471003, People's Republic of China*
[17]*Huangshan College, Huangshan 245000, People's Republic of China*
[18]*Hunan University, Changsha 410082, People's Republic of China*
[19]*Indiana University, Bloomington, Indiana 47405, USA*
[20a]*INFN Laboratori Nazionali di Frascati, I-00044 Frascati, Italy*
[20b]*INFN and University of Perugia, I-06100, Perugia, Italy*
[21a]*INFN Sezione di Ferrara, I-44122 Ferrara, Italy*
[21b]*University of Ferrara, I-44122 Ferrara, Italy*
[22]*Johannes Gutenberg University of Mainz, Johann-Joachim-Becher-Weg 45, D-55099 Mainz, Germany*
[23]*Joint Institute for Nuclear Research, 141980 Dubna, Moscow Region, Russia*
[24]*Justus Liebig University Giessen, II. Physikalisches Institut, Heinrich-Buff-Ring 16,
D-35392 Giessen, Germany*
[25]*KVI-CART, University of Groningen, NL-9747 AA Groningen, The Netherlands*
[26]*Lanzhou University, Lanzhou 730000, People's Republic of China*
[27]*Liaoning University, Shenyang 110036, People's Republic of China*
[28]*Nanjing Normal University, Nanjing 210023, People's Republic of China*
[29]*Nanjing University, Nanjing 210093, People's Republic of China*
[30]*Nankai University, Tianjin 300071, People's Republic of China*
[31]*Peking University, Beijing 100871, People's Republic of China*
[32]*Seoul National University, Seoul 151-747, Korea*
[33]*Shandong University, Jinan 250100, People's Republic of China*
[34]*Shanghai Jiao Tong University, Shanghai 200240, People's Republic of China*
[35]*Shanxi University, Taiyuan 030006, People's Republic of China*
[36]*Sichuan University, Chengdu 610064, People's Republic of China*
[37]*Soochow University, Suzhou 215006, People's Republic of China*
[38]*Sun Yat-Sen University, Guangzhou 510275, People's Republic of China*
[39]*Tsinghua University, Beijing 100084, People's Republic of China*
[40a]*Istanbul Aydin University, 34295 Sefakoy, Istanbul, Turkey*
[40b]*Dogus University, 34722 Istanbul, Turkey*
[40c]*Uludag University, 16059 Bursa, Turkey*
[41]*University of Chinese Academy of Sciences, Beijing 100049, People's Republic of China*
[42]*University of Hawaii, Honolulu, Hawaii 96822, USA*
[43]*University of Minnesota, Minneapolis, Minnesota 55455, USA*
[44]*University of Rochester, Rochester, New York 14627, USA*
[45]*University of Science and Technology of China, Hefei 230026, People's Republic of China*
[46]*University of South China, Hengyang 421001, People's Republic of China*
[47]*University of the Punjab, Lahore 54590, Pakistan*
[48a]*University of Turin, I-10125 Turin, Italy*
[48b]*University of Eastern Piedmont, I-15121 Alessandria, Italy*
[48c]*INFN, I-10125 Turin, Italy*
[49]*Uppsala University, Box 516, SE-75120 Uppsala, Sweden*
[50]*Wuhan University, Wuhan 430072, People's Republic of China*

[51]*Zhejiang University, Hangzhou 310027, People's Republic of China*
[52]*Zhengzhou University, Zhengzhou 450001, People's Republic of China*
[53]*Center for Exploration of Energy and Matter, Indiana University, Bloomington, Indiana 47403, USA*
[54]*Theory Center, Thomas Jefferson National Accelerator Facility, Newport News, Virginia 23606, USA*

An amplitude analysis of the $\pi^0\pi^0$ system produced in radiative J/ψ decays is presented. In particular, a piecewise function that describes the dynamics of the $\pi^0\pi^0$ system is determined as a function of $M_{\pi^0\pi^0}$ from an analysis of the $(1.311 \pm 0.011) \times 10^9$ J/ψ decays collected by the BESIII detector. The goal of this analysis is to provide a description of the scalar and tensor components of the $\pi^0\pi^0$ system while making minimal assumptions about the properties or number of poles in the amplitude. Such a model-independent description allows one to integrate these results with other related results from complementary reactions in the development of phenomenological models, which can then be used to directly fit experimental data to obtain parameters of interest. The branching fraction of $J/\psi \rightarrow \gamma\pi^0\pi^0$ is determined to be $(1.15 \pm 0.05) \times 10^{-3}$, where the uncertainty is systematic only and the statistical uncertainty is negligible.

I. INTRODUCTION

While the Standard Model of particle physics has yielded remarkable successes, the connection between quantum chromodynamics (QCD) and the complex structure of hadron dynamics remains elusive. The light isoscalar scalar meson spectrum ($I^G J^{PC} = 0^+ 0^{++}$), for example, remains relatively poorly understood despite many years of investigation. This lack of understanding is due in part to the presence of broad, overlapping states, which are poorly described by the most accessible analytical methods [see the "Note on scalar mesons below 2 GeV" from the Particle Data Group (PDG) [1]]. The PDG reports eight $0^+ 0^{++}$ mesons, which have widths between 100 and 450 MeV. Several of these states, including the $f_0(1370)$, are characterized in the PDG only by ranges of values for their masses and widths.

Knowledge of the low mass scalar meson spectrum is important for several reasons. In particular, the lightest glueball state is expected to have scalar quantum numbers [2–5]. The existence of such a state is an excellent test of QCD. Experimental observation of a glueball state would provide evidence that gluon self-interactions can generate a massive meson. Unfortunately, glueballs may mix with conventional quark bound states, making the identification of glueball states experimentally challenging. The low mass scalar meson spectrum is also of interest in probing the fundamental interactions of hadrons in that it allows for testing of chiral perturbation theory to one loop [6].

The scalar meson spectrum has been studied in many reactions, including πN scattering [7], $p\bar{p}$ annihilation [8], central hadronic production [9], decays of the ψ' [10], J/ψ [11–13], B [14], D [15], and K [16] mesons, $\gamma\gamma$ formation [17], and ϕ radiative decays [18]. In particular, a coupled channel analysis using the K-matrix formalism has been performed using data from pion production, $p\bar{p}$ and $n\bar{p}$ annihilation, and $\pi\pi$ scattering [19]. Similar investigations would benefit from the inclusion of data from radiative J/ψ decays, which provide a complementary source of hadronic production.

An attractive feature of a study of the two pseudoscalar spectra in radiative J/ψ decays is the relative simplicity of the amplitude analysis. Conservation of parity in strong and electromagnetic interactions, along with the conservation of angular momentum, restricts the quantum numbers of the pseudoscalar-pseudoscalar pair. Only amplitudes with even angular momentum and positive parity and charge conjugation quantum numbers are accessible ($J^{PC} = 0^{++}$, 2^{++}, 4^{++}, etc.). Initial studies suggest that only the 0^{++} and 2^{++} amplitudes are significant in radiative J/ψ decays to $\pi^0\pi^0$. The neutral channel ($\pi^0\pi^0$) is of particular interest due to the lack of sizable backgrounds like $\rho\pi$, which present a challenge for an analysis of the charged channel ($\pi^+\pi^-$) [20].

Radiative J/ψ decays to $\pi^+\pi^-$ have been analyzed previously by the MarkIII [21], DM2 [22], and BES [23] experiments. Decays to $\pi^0\pi^0$ were also studied at Crystal Ball [24] and BES [25], but these analyses were severely limited by statistics, particularly for the higher mass states. Each of these analyses reported evidence for

---

[a]Also at State Key Laboratory of Particle Detection and Electronics, Beijing 100049, Hefei 230026, People's Republic of China.
[b]Also at Ankara University, 06100 Tandogan, Ankara, Turkey.
[c]Also at Bogazici University, 34342 Istanbul, Turkey.
[d]Also at the Moscow Institute of Physics and Technology, Moscow 141700, Russia.
[e]Also at the Functional Electronics Laboratory, Tomsk State University, Tomsk 634050, Russia.
[f]Also at the Novosibirsk State University, Novosibirsk 630090, Russia.
[g]Also at the NRC Kurchatov Institute, PNPI, 188300, Gatchina, Russia.
[h]Also at University of Texas at Dallas, Richardson, Texas 75083, USA.
[i]Present address: Istanbul Arel University, 34295 Istanbul, Turkey.

the $f_2(1270)$ and some possible additional states near 1.710 GeV/c^2 and 2.050 GeV/c^2. More recently, the BESII experiment studied these channels and implemented a partial wave analysis [20]. Prominent features in the results include the $f_2(1270)$, $f_0(1500)$, and $f_0(1710)$. However, this analysis, like its predecessors, was limited by complications from large backgrounds and low statistics. Due to statistical limitations, the $\pi^0\pi^0$ channel was used only as a cross-check on the analysis of the charged channel.

Historically, amplitude analyses like that in Ref. [20] have relied on modeling the s-dependence of the $\pi\pi$ interaction, where s is the invariant mass squared of the two pions, as a coherent sum of resonances, each described by a Breit-Wigner function. In doing so, a model is built whose parameters are resonance properties, e.g., masses, widths, and branching fractions. A correspondence exists between these properties and the residues and poles of the $\pi\pi$ scattering amplitude in the complex s plane; however, this correspondence is valid only in the limit of an isolated narrow resonance that is far from open thresholds (cf. Ref. [1]). For regions containing multiple overlapping resonances with large widths and the presence of thresholds, all of which occur in the 0^{++} $\pi\pi$ spectrum, an amplitude constructed from a sum of Breit-Wigner functions becomes an approximation. While such an approximation provides a practical and controlled way to parametrize the data—additional resonances can be added to the sum until an adequate fit is achieved—it is unknown how well it maintains the correspondence between Breit-Wigner parameters and the analytic structure of the $\pi\pi$ amplitude that one seeks to study, i.e., the fundamental strong interaction physics. Often statistical precision, a lack of complementary constraining data, or a limited availability of models leaves the simple Briet-Wigner sum as a necessary but untested assumption in analyses, thereby rendering the numerical result useful only in the context of that assumption. In the context of this paper we refer to the Breit-Wigner sum as a "mass dependent fit"; that is, the model used to fit the data has an assumed s dependence.

In this analysis we exploit the statistical precision provided by $(1.311 \pm 0.011) \times 10^9$ J/ψ decays collected with the BESIII detector [26,27] to measure the components of the $\pi\pi$ amplitude independently for many small regions of $\pi\pi$ invariant mass, which allows one to construct a piecewise complex function from the measurements that describes the s-dependence of the $\pi\pi$ dynamics. Such a construction makes minimal assumptions about the s-dependence of the $\pi\pi$ interaction. We refer to this approach in the context of the paper as a "mass independent fit."

The mass independent approach has some drawbacks. First, because of the large number of bins, one is left with a set of about a thousand parameters that describe the amplitudes with no single parameter tied to an individual resonance of interest. Second, mathematical ambiguities

result in multiple sets of optimal parameters in each mass region. If only $J = 0$ and $J = 2$ resonances are significant, there are two ambiguous solutions. However, in general, if one includes $J \geq 4$, the number of ambiguous solutions increases resulting in multiple allowed piecewise functions. Finally, in order to make the results practically manageable for subsequent analysis, the assumption of Gaussian errors must be made—an assumption that cannot be validated in general. Similar limitations are present in other analyses of this type, e.g., Ref. [7]. In spite of these limitations, which are discussed further in Appendixes B and C, the results of the mass independent amplitude analysis presented here represent a measurement of $\pi\pi$ dynamics in radiative J/ψ decays that minimizes experimental artifacts and potential systematic biases due to theoretical assumptions. The results are presented with the intent of motivating the development of dynamical models with reaction independent parameters that can subsequently be optimized using experimental data. All pertinent information for the use of these results in the study of pseudoscalar-pseudoscalar dynamics is included in the supplemental materials (Appendix C).

II. THE BESIII DETECTOR

The Beijing Spectrometer (BESIII) is a general-purpose, hermetic detector located at the Beijing Electron-Positron Collider (BEPCII) in Beijing, China. BESIII and BEPCII represent major upgrades to the BESII detector and BEPC accelerator. The physics goals of the BESIII experiment cover a broad research program including charmonium physics, charm physics, light hadron spectroscopy, and τ physics, as well as searches for physics beyond the standard model. The detector is described in detail elsewhere [28]. A brief description follows.

The BESIII detector consists of five primary components working in conjunction to facilitate the reconstruction of events. A superconducting solenoid magnet provides a uniform magnetic field within the detector. The field strength was 1.0 T during data collection in 2009, but was reduced to 0.9 T during the 2012 running period. Charged particle tracking is performed with a helium-gas based multilayer drift chamber (MDC). The momentum resolution of the MDC is expected to be better than 0.5% at 1 GeV/c, while the expected dE/dx resolution is 6%. With a timing resolution of 80 ps (110 ps) in the barrel (end cap), a plastic scintillator time-of-flight detector is useful for particle identification. The energies of electromagnetic showers are determined using information from the electromagnetic calorimeter (EMC). The EMC consists of 6240 CsI(Tl) crystals arranged in one barrel and two end cap sections. With an angular coverage of about 93% of 4π, the EMC provides an energy resolution of 2.5% (5%) at 1.0 GeV and a position resolution of 6 mm (9 mm) in the barrel (end cap). Finally, particles that escape these detectors travel through a muon chamber system (MUC),

TABLE I. The number of events remaining after all selection criteria for each of a number of background reactions is shown in the right column. The backgrounds are broken into three groups. The first group contains the signal mimicking decays. The second lists the remaining backgrounds from J/ψ decays to $\gamma\eta(')$, while the third group lists a few additional backgrounds. The backgrounds explicitly listed here represent about 93% of the total background according to the MC samples. The misreconstructed background includes those events in which one of the daughter photons from a π^0 decay is taken as the radiated photon.

Decay channel	Number of events
$J/\psi \to \gamma\pi^0\pi^0$ (data)	442,562
$e^+e^- \to \gamma\pi^0\pi^0$ (continuum)	3,632
$J/\psi \to b_1\pi^0; b_1 \to \gamma\pi^0$	1,606
$J/\psi \to \omega\pi^0; \omega \to \gamma\pi^0$	865
$J/\psi \to \rho\pi^0; \rho \to \gamma\pi^0$	778
Misreconstructed background	608
$J/\psi \to \gamma\eta; \eta \to 3\pi^0$	903
$J/\psi \to \gamma\eta'; \eta' \to \eta\pi^0\pi^0; \eta \to \gamma\gamma$	377
$J/\psi \to \omega\pi^0\pi^0; \omega \to \gamma\pi^0$	775
$J/\psi \to b_1\pi^0; b_1 \to \omega\pi^0; \omega \to \gamma\pi^0$	578
$J/\psi \to \omega\eta; \omega \to \gamma\pi^0$	409
$J/\psi \to \omega f_2(1270); \omega \to \gamma\pi^0$	299
$J/\psi \to \gamma\eta_c; \eta_c \to \gamma\pi^0\pi^0 \, or \, \pi^0\pi^0\pi^0$	255
Other backgrounds	507
Total background (MC)	7,960

which provides additional information on the identity of particles. The MUC provides 2 cm position resolution for muons and covers 89% of 4π. Muons with momenta over 0.5 GeV are detected with an efficiency greater than 90%.

The efficiency of pions reaching the MUC is about 10% at this energy.

Selection criteria and background estimations are studied using a GEANT4 Monte Carlo (MC) simulation. The BESIII Object Oriented Simulation Tool (BOOST) [29] provides a description of the geometry, material composition, and detector response of the BESIII detector. The MC generator KKMC [30] is used for the production of J/ψ mesons by e^+e^- annihilation, while BESEVTGEN [31] is used to generate the known decays of the J/ψ according to the world average values from the PDG [1]. The unknown portion of the J/ψ decay spectrum is generated with the Lundcharm model [32].

III. EVENT SELECTION

In order to be included in the amplitude analysis, an event must have at least five photon candidates and no charged track candidates. Any photon detected in the barrel (end cap) portion of the EMC must have an energy of at least 25 (50) MeV. Four of the five photons are grouped into two pairs that may each originate from a π^0 decay. The invariant mass of any photon pair associated with a π^0 must fall within 13 MeV/c^2 of the π^0 mass. A 6C kinematic fit is performed on each permutation of photons to the final state $\gamma\pi^0\pi^0$. This includes a constraint on the four-momentum of the final state to that of the initial J/ψ (4C) and an additional constraint (1C) on each photon pair to have an invariant mass equal to that of a π^0.

Significant backgrounds in this channel include J/ψ decays to $\gamma\eta$ ($\eta \to \pi^0\pi^0\pi^0$) and $\gamma\eta'$ ($\eta' \to \eta\pi^0\pi^0; \eta \to \gamma\gamma$). Restricting the χ^2 from the 6C kinematic fit is an effective means of reducing the backgrounds of this type. Events with a $\pi^0\pi^0$ invariant mass, $M_{\pi^0\pi^0}$, below the KK threshold (the
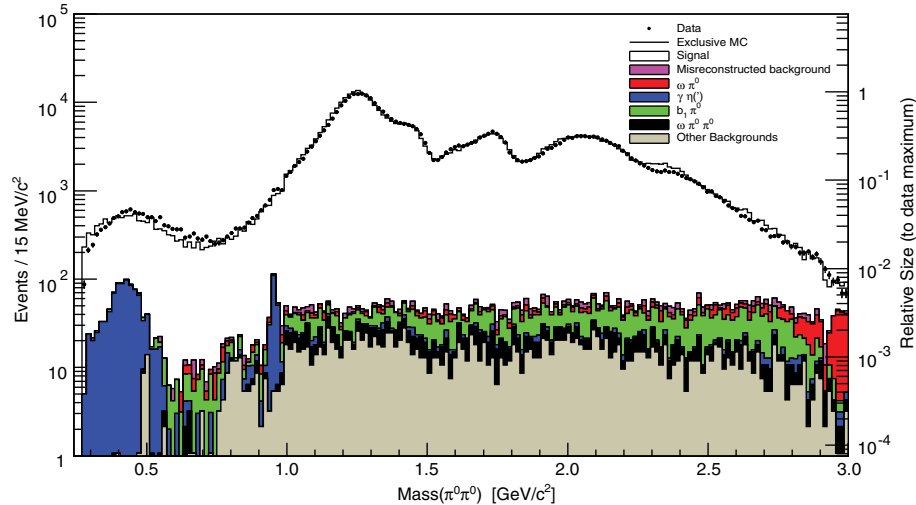
FIG. 1 (color online). The $M_{\pi^0\pi^0}$ spectrum after all selection criteria have been applied. The black markers represent the data, while the histograms depict the backgrounds according to the MC samples. The signal (white) and misreconstructed background (pink) are determined from an exclusive MC sample that resembles the data. The other backgrounds are determined from an inclusive MC sample (see Table I). The components of the stacked histogram from bottom up are unspecified backgrounds, $\omega\pi^0\pi^0$, $b_1\pi^0$, $\gamma\eta(')$, $\omega\pi^0$, the misreconstructed background, and the signal.

region in which these backgrounds are significant) must have a χ^2 less than 20. Events above the KK threshold need only have a χ^2 less than 60. To reduce the background from J/ψ decays to $\omega\pi^0$ ($\omega \to \gamma\pi^0$), the invariant mass of each $\gamma\pi^0$ pair is required to be at least 50 MeV/c^2 away from the ω mass [1]. Finally, in order to reduce the misreconstructed background arising from pairing the radiated photon with another photon in the event to form a π^0, the invariant mass of the radiated photon paired with any π^0 daughter photon is required to be greater than 0.15 GeV/c^2.

If more than one permutation of five photons in an event satisfy these selection criteria, only the permutation with the minimum χ^2 from the 6C kinematic fit is retained. After all event selection criteria are applied, the number of events remaining in the data sample is 442,562. MC studies indicate that the remaining backgrounds exist at a level of about 1.8% of the size of the total sample. Table I lists the major backgrounds.

Backgrounds from J/ψ decays to $\gamma\eta(\prime)$ are well understood and are studied with an exclusive MC sample, which is generated according to the PDG branching fractions for these reactions. Other backgrounds are studied using an inclusive MC sample generated using BESEVTGEN, with the exception of the misreconstructed background, which is studied using an exclusive MC sample that resembles the data. The latter MC sample was generated using a set of Breit-Wigner resonances with couplings determined from a mass dependent fit to the data sample. The $M_{\pi^0\pi^0}$ spectrum after all selection criteria have been applied is shown in Fig. 1. The reconstruction efficiency is determined to be 28.7%, according to the results of the mass independent amplitude analysis. Continuum backgrounds are investigated with a data sample collected at a center of mass energy of 3.080 GeV. The continuum backgrounds are scaled by luminosity and a correction factor for the difference in cross section as a function of center of mass energy. When scaled by luminosity, only 3,632 events, which represents approximately 0.8% of the signal, survive after all signal isolation requirements.

IV. AMPLITUDE ANALYSIS

A. General formalism

The results of the mass independent amplitude analysis of the $\pi^0\pi^0$ system are obtained from a series of unbinned extended maximum likelihood fits. The amplitudes for radiative J/ψ decays to $\pi^0\pi^0$ are constructed in the radiative multipole basis, as described in detail in Appendix A.

Let U^{M,λ_γ} represent the amplitude for radiative J/ψ decays to $\pi^0\pi^0$,

$$U^{M,\lambda_\gamma}(\vec{x}, s) = \langle\gamma\pi^0\pi^0|H|J/\psi\rangle, \qquad (1)$$

where $\vec{x} = \{\theta_\gamma, \phi_\gamma, \theta_\pi, \phi_\pi\}$ is the position in phase space, $s = M^2_{\pi^0\pi^0}$ is the invariant mass squared of the $\pi^0\pi^0$ pair, M is the polarization of the J/ψ, and λ_γ is the helicity of the radiated photon. For the reaction under study the possible values of both M and λ_γ are ±1. The amplitude may be factorized into a piece that contains the radiative transition of the J/ψ to an intermediate state X and a piece that contains the QCD dynamics

$$U^{M,\lambda_\gamma}(\vec{x}, s) = \sum_{j,J_\gamma,X}\langle\pi^0\pi^0|H_{\text{QCD}}|X_{j,J_\gamma}\rangle$$
$$\times \langle\gamma X_{j,J_\gamma}|H_{EM}|J/\psi\rangle, \qquad (2)$$

where j is the angular momentum of the intermediate state and J_γ indexes the radiative multipole transitions. The sum over X includes any pseudoscalar-pseudoscalar final states ($\pi\pi$, $K\bar{K}$, etc.) that may rescatter into $\pi^0\pi^0$. We assume that the contribution of the 4π final state to this sum is negligible, with the result that rescattering effects become important only above the $K\bar{K}$ threshold.

The amplitude in Eq. (2) may be further factorized by pulling out the angular distributions,

$$U^{M,\lambda_\gamma}(\vec{x}, s) = \sum_{j,J_\gamma,X}T_{j,X}(s)\Theta^{M,\lambda_\gamma}_j(\theta_\pi, \phi_\pi)$$
$$\times g_{j,J_\gamma,X}(s)\Phi^{M,\lambda_\gamma}_{j,J_\gamma}(\theta_\gamma, \phi_\gamma), \qquad (3)$$

where $g_{j,J_\gamma,X}(s)$ is the coupling for the radiative decay to intermediate state X. The functions $\Theta^{M,\lambda_\gamma}_j(\theta_\pi, \phi_\pi)$ and $\Phi^{M,\lambda_\gamma}_{j,J_\gamma}(\theta_\gamma, \phi_\gamma)$ contain the angular dependence of the decay of the X to $\pi^0\pi^0$ and the radiative J/ψ decay, respectively. The part of the amplitude that describes the $\pi^0\pi^0$ dynamics is the complex function $T_{j,X}(s)$, which is of greatest interest for this study. However, this function cannot be separated from the coupling $g_{j,J_\gamma,X}(s)$. Instead the product is measured according to

$$V_{j,J_\gamma}(s) \approx \sum_X g_{j,J_\gamma,X}(s)T_{j,X}(s). \qquad (4)$$

This product will be called the coupling to the state with characteristics j, J_γ. Note here that, if rescattering effects are assumed to be minimal (the only possible X is $\pi\pi$), all amplitudes with the same j have the same phase. The effect of rescattering is to break the factorizability of Eq. (4). Finally, the amplitude may be written

$$U^{M,\lambda_\gamma}(\vec{x}, s) = \sum_{j,J_\gamma}V_{j,J_\gamma}(s)A^{M,\lambda_\gamma}_{j,J_\gamma}(\vec{x}), \qquad (5)$$

where $A^{M,\lambda_\gamma}_{j,J_\gamma}(\vec{x})$ contains the piece of the amplitude that describes the angular distributions and is determined by the kinematics of an event.

Any amplitude with total angular momentum greater than zero will have three components (the 0^{++} amplitude has only an E1 component). Thus, three 2^{++} amplitudes, relating to E1, M2, and E3 radiative transitions, are included in the analysis. While any amplitude with even total angular momentum and positive parity and charge conjugation is accessible for this decay, studies show that the 4^{++} amplitude is not significant in this region. In particular, no set of four continuous 15 MeV/c^2 bins yield a difference in $-2\ln L$ greater than 28.8 units, which corresponds to a five sigma difference, under the inclusion of a 4^{++} amplitude. As no narrow spin-4 states are known, this suggests that only the 0^{++} and 2^{++} amplitudes are significant. The systematic uncertainty due to ignoring a 4^{++} amplitude that may exist in the data is described below in Sec. V C.

B. Parametrization

The dynamical function in Eq. (4) may be parametrized in various ways. A common parametrization, discussed in the Introduction, is a sum of interfering Breit-Wigner functions,

$$V_{j,J_\gamma}(s) = \sum_\beta k_{j,J_\gamma,\beta} \mathrm{BW}_{j,J_\gamma,\beta}(s), \qquad (6)$$

where $\mathrm{BW}_{j,J_\gamma,\beta}(s)$ represents a Breit-Wigner function with characteristics (mass and width) β and strength $k_{j,J_\gamma,\beta}$.

To avoid making such a strong model dependent assumption, we choose to bin the data sample as a function of $M_{\pi^0\pi^0}$ and to assume that the part of the amplitude that describes the dynamical function is constant over a small range of s,

$$U^{M,\lambda_\gamma}(\vec{x},s) = \sum_{j,J_\gamma} V_{j,J_\gamma} A_{j,J_\gamma}^{M,\lambda_\gamma}(\vec{x}). \qquad (7)$$

For the scenario posed in Eq. (7), the couplings may be taken as the free parameters of an extended maximum likelihood fit in each bin of $M_{\pi^0\pi^0}$. It is then possible to extract a table of complex numbers (the free parameters in each bin) that describe the dynamical function of the $\pi^0\pi^0$ interaction.

The intensity function, $I(\vec{x})$, which represents the density of events at some position in phase space $\vec{x}$, is given by

$$I(\vec{x}) = \sum_{M,\lambda_\gamma} \left| \sum_{j,J_\gamma} V_{j,J_\gamma} A_{j,J_\gamma}^{M,\lambda_\gamma}(\vec{x}) \right|^2. \qquad (8)$$

The incoherent sum includes the observables of the reaction (which are not measured). For the reaction under study, the observables are the polarization of the J/ψ, $M = \pm 1$, and the helicity of the radiated photon, $\lambda_\gamma = \pm 1$. The free parameters are constrained to be the same in each of the four pieces of the incoherent sum.

In the figures and supplemental results that follow, the intensity of the amplitude in each bin is reported as a number of events corrected for acceptance and detector efficiency. That is, for the bin of $M_{\pi^0\pi^0}$ indexed by k and bounded by s_k and s_{k+1} (the boundaries in s of the bin) we report, for each amplitude indexed by j and J_γ, the quantity

$$I_{j,J_\gamma}^k = \int_{s_k}^{s_{k+1}} \sum_{M,\lambda_\gamma} \left| V_{j,J_\gamma}^k A_{j,J_\gamma}^{M,\lambda_\gamma}(\vec{x}) \right|^2 d\vec{x}. \qquad (9)$$

In practice, we absorb the size of phase space into the fit parameters. In doing so we fit for parameters $\tilde{V}_{j,J_\gamma}^k$ which are the V_{j,J_γ}^k scaled by the square root of the size of phase space in bin k.

C. Background subtraction

The mass independent amplitude analysis treats each event in the data sample as a signal event. For a clean sample, the effect of remaining backgrounds should be small relative to the statistical errors on the amplitudes. However, the backgrounds from J/ψ decays to $\gamma\eta(')$ introduce a challenge. Both of these backgrounds peak in the low mass region near interesting structures. The background from J/ψ decays to $\gamma\eta$ lies in the region of the $f_0(500)$, which is of particular interest for its importance to chiral perturbation theory [1,33]. The $\gamma\eta'$ background peaks near the $f_0(980)$, which is also of particular interest due to its strong coupling to $K\bar{K}$ and its implications for a scalar meson nonet [34]. Therefore, the effect of these backgrounds is removed by using a background subtraction method.

If a data sample is entirely free of backgrounds, the likelihood function is constructed as

$$L(\vec{\xi}) = \prod_{i=1}^{N_{\mathrm{data}}^{\mathrm{sig}}} f(\vec{x}_i|\vec{\xi}), \qquad (10)$$

where $f(\vec{x}|\vec{\xi})$ is the probability density function to observe an event with a particular set of kinematics $\vec{x}$ and parameters $\vec{\xi} = \{\tilde{V}_{j,J_\gamma}^k\}$. The total number of parameters in the mass independent analysis is 1,178 (7 times the number of bins above $K\bar{K}$ threshold and 5 times the number of bins below $K\bar{K}$ threshold). The number of events in the pure data sample is given by $N_{\mathrm{data}}^{\mathrm{sig}}$.

Now, the likelihood may be written

$$L(\vec{\xi}) = \prod_{i=1}^{N_{\mathrm{data}}^{\mathrm{sig}}} f(\vec{x}_i|\vec{\xi}) \prod_{j=1}^{N_{\mathrm{data}}^{\mathrm{bkg}}} f(\vec{x}_j|\vec{\xi}) \prod_{k=1}^{N_{\mathrm{data}}^{\mathrm{bkg}}} f(\vec{x}_k|\vec{\xi})^{-1}, \qquad (11)$$

where an additional likelihood, which describes the reaction for background events, has been multiplied and

divided. Consider now a more realistic data sample that not only consists of signal events but also contains some number of background events, $N_{\mathrm{data}}^{\mathrm{bkg}}$. Then the product of the first two factors of Eq. (11) are simply the likelihood for the entire (contaminated) data sample, but the overall likelihood represents only that of the pure signal since the background likelihood has been divided. For a given data set, any backgrounds remaining after selection criteria have been applied are difficult to distinguish from the true signal. Rather than using the true background to determine the background likelihood, it is therefore necessary to approximate it with an exclusive MC sample. That is,

$$\prod_{i=1}^{N_{\mathrm{data}}^{\mathrm{bkg}}} f(\vec{x}_i|\vec{\xi})^{-1} \approx \prod_{i=1}^{N_{\mathrm{MC}}^{\mathrm{bkg}}} f(\vec{x}_i|\vec{\xi})^{-w_i}, \qquad (12)$$

where the weight, w_i, is necessary for scaling purposes. For example, if the MC sample is twice the size of the expected background, a weight factor of 0.5 is necessary. Finally, the likelihood function may be written

$$L(\vec{\xi}) = \prod_{i=1}^{N_{\mathrm{data}}} f(\vec{x}_i|\vec{\xi}) \prod_{j=1}^{N_{\mathrm{MC}}^{\mathrm{bkg}}} f(\vec{x}_j|\vec{\xi})^{-w_j}. \qquad (13)$$

In practice, this likelihood distribution is multiplied by a Poisson distribution for the extended maximum likelihood fits such that

$$L(\vec{\xi}) = \frac{e^{-\mu}\mu^{N_{\mathrm{data}}}}{N_{\mathrm{data}}!} \prod_{i=1}^{N_{\mathrm{data}}} f(\vec{x}_i|\vec{\xi}) \prod_{j=1}^{N_{\mathrm{MC}}^{\mathrm{bkg}}} f(\vec{x}_j|\vec{\xi})^{-w_j}. \qquad (14)$$

An exclusive MC sample for the backgrounds due to J/ψ decays to $\gamma\eta(')$ is generated according to the branching fractions given by the PDG [1]. This MC sample is required to pass all of the selection criteria that are applied to the data sample. Any events that remain are included in the unbinned extended maximum likelihood fit with a negative weight $[-w_j = -1$ in Eq. (13)]. In this way, the inclusion of the MC sample in the fit approximately cancels the effect of any remaining backgrounds of the same type in the data sample.

D. Ambiguities

Another challenge to the amplitude analysis is the presence of ambiguities. Since the intensity function, which is fit to the data, is constructed from a sum of absolute squares, it is possible to identify multiple sets of amplitudes which give identical values for the total intensity. In this way, multiple solutions may give comparable values of $-2\ln L$ for a particular fit. For this particular analysis, two types of ambiguities are present. Trivial ambiguities arise due to the possibility of the overall amplitude in each bin to be rotated by π or to be reflected over the real axis in the complex plane. These may be partially addressed by

applying a phase convention to the results of the fits. Nontrivial ambiguities arise from the freedom of amplitudes with the same quantum numbers to have different phases. The nontrivial ambiguities represent a greater challenge to the analysis and cannot be eliminated without introducing model dependencies.

While it is not possible in principle to measure the absolute phase of the amplitudes, it is possible to study the relative phases of individual amplitudes. Therefore in each of the fits, one of the amplitudes (the 2^{++} E1 amplitude) is constrained to be real. The phase difference between the other amplitudes and that which is constrained can then be determined in each mass bin.

As mentioned above, a set of trivial ambiguities arises due to the possibility of the overall amplitude in each bin to be rotated by π or to be reflected over the real axis in the complex plane. Each of these processes leaves the intensity distribution unchanged. This issue is partially resolved by establishing a phase convention in which the amplitude that is constrained to be real is also constrained to be positive. The remaining ambiguity is related to the inability to determine the absolute phase. The phase of the total amplitude may change sign without inducing a change in the total intensity. Therefore, when a phase difference approaches zero, it is not possible to determine if the phase difference should change sign. The amplitude analysis results are presented here with the arbitrary convention that the phase difference between the 0^{++} amplitude and the 2^{++} E1 amplitude is required to be positive. One may invert the sign of this phase difference in a given bin, but then all other phase differences in that bin must also be inverted.

The presence of nontrivial ambiguities is attributed to rescattering effects, which allow for amplitudes with the same quantum numbers, J^{PC}, to have different phases. The couplings, $g_{j,J_\gamma,X}(s)$, in Eq. (4) are real functions of s. Since the dynamical amplitude, $T_{j,X}(s)$, does not depend on J_γ, its phase is the same for each of the amplitudes with the same J^{PC} (in particular, the 2^{++} E1, M2, and E3 amplitudes). However, if more than one intermediate state, X, is present, differences between the couplings to these amplitudes may result in a phase difference. Therefore, in the region above the $K\bar{K}$ threshold the 2^{++} amplitudes may have different phases. However, below the $K\bar{K}$ threshold the phases of these amplitudes are constrained to be the same. That is, rescattering through 4π is assumed to be negligible.

By writing out the angular dependence of the intensity function, it is possible to show that the freedom to have phase differences between the components of a given amplitude (2^{++} E1, M2, and E3, for example) generates an ambiguity in the intensity distribution. For this channel and considering only 0^{++} and 2^{++} amplitudes, two nontrivial ambiguous solutions may be present in each bin above the $K\bar{K}$ threshold. The knowledge of one solution can be used to mathematically predict its ambiguous partner. In fact, some bins do not exhibit multiple solutions,

but have a degenerate ambiguous pair. A study of these ambiguities (Appendix B) shows consistency between the mathematically predicted and experimentally determined ambiguities. Both ambiguous solutions are presented, because it is impossible to know which represent the physical solutions without making some additional model dependent assumptions. If more than two solutions are found in a given bin, all solutions within 1 unit of log likelihood from the best solution are compared to the predicted value *derived from the best solution* and only that which matches the prediction is accepted as the ambiguous partner.
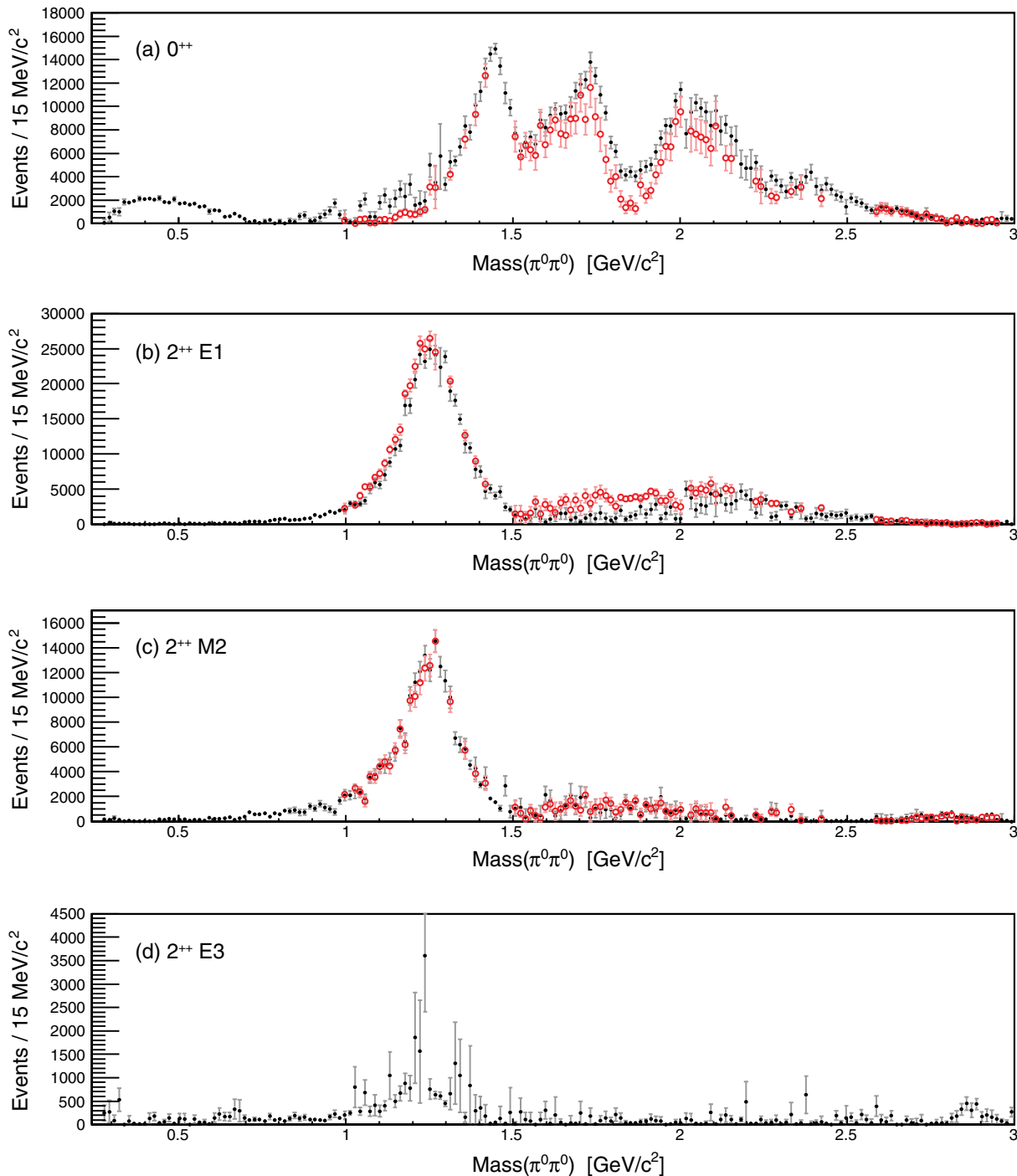
FIG. 2 (color online). The intensities for the (a) 0^{++}, (b) 2^{++} E1, (c) 2^{++} M2, and (d) 2^{++} E3 amplitudes as a function of $M_{\pi^0\pi^0}$ for the nominal results. The solid black markers show the intensity calculated from one set of solutions, while the open red markers represent its ambiguous partner. Note that the intensity of the 2^{++} E3 amplitude is redundant for the two ambiguous solutions (see Appendix B). Only statistical errors are presented.

E. Results

1. Amplitude intensities and phases

The intensity for each amplitude as a function of $M_{\pi^0\pi^0}$ is plotted in Fig. 2. Each of the phase differences with respect to the reference amplitude (2^{++} E1), which is constrained to be real, is plotted in Fig. 3. Above the $K\bar{K}$ threshold, two distinct sets of solutions are apparent in most bins as expected. The bins below about 0.6 GeV/c^2 also contain multiple solutions, but with different likelihoods and are attributed to local minima in the likelihood function. The nominal solutions below 0.6 GeV/c^2 are determined by requiring continuity in each intensity and phase difference as a function of $M_{\pi^0\pi^0}$. Only statistical errors are presented in the figures.

It is apparent that the ambiguous sets of solutions in the nominal results are distinct in some regions, while they

approach and possibly cross at other points. The most powerful discriminator of this effect is the phase difference between the E1 and M2 components of the 2^{++} amplitude (see the middle plot of Fig. 3). Regions in which the solutions may cross are apparent at 0.99 GeV/c^2, near 1.3 GeV/c^2, and above 2.3 GeV/c^2. Since the results in each bin are independent of their neighbor, it is not possible to identify two distinct, smooth solutions at these crossings.

2. Discussion

The results of the mass independent analysis exhibit significant structures in the 0^{++} amplitude just below 1.5 GeV/c^2 and near 1.7 GeV/c^2. This region is where one might expect to observe the states $f_0(1370)$, $f_0(1500)$, and $f_0(1710)$ which are often cited as being mixtures of
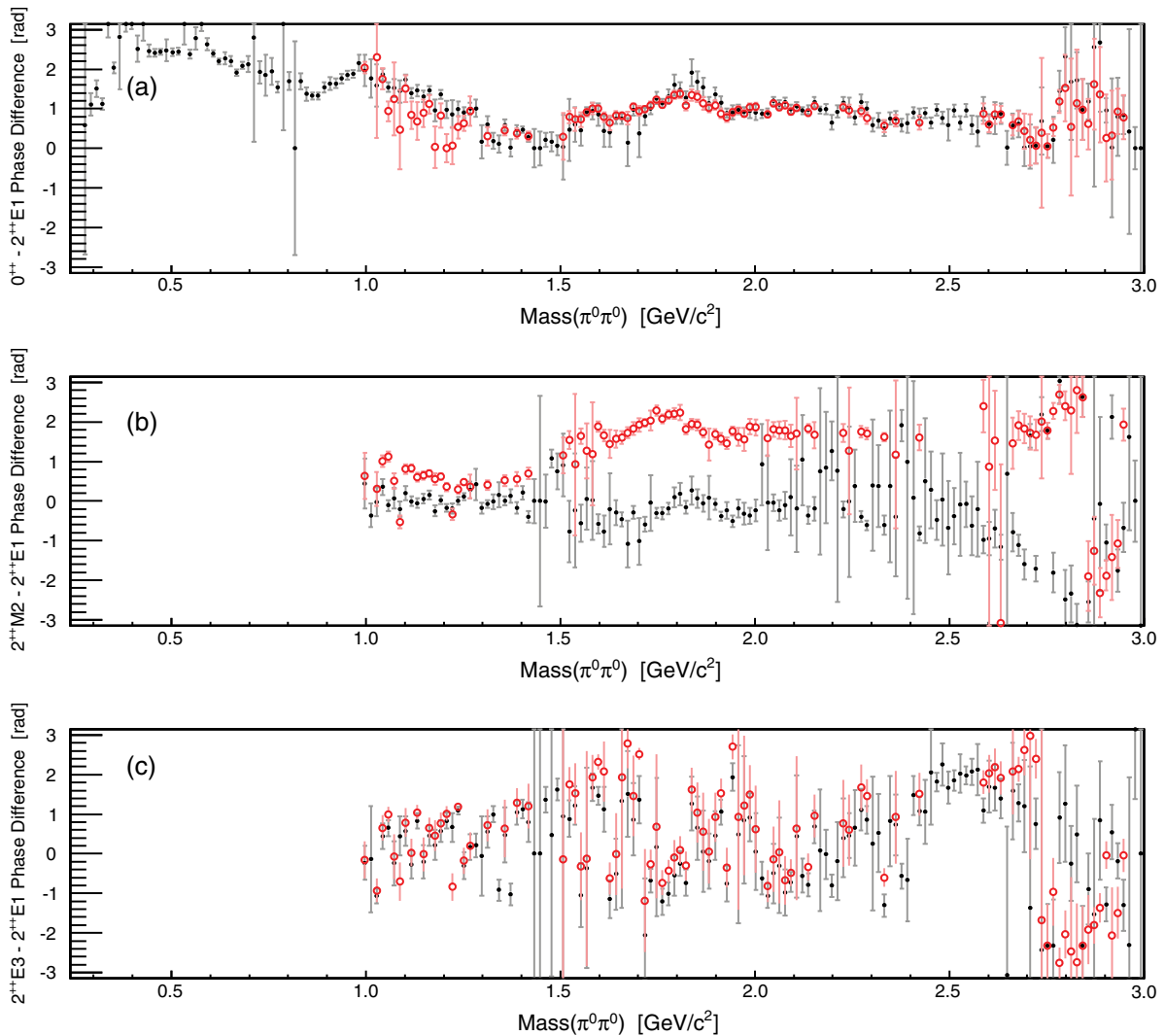
FIG. 3 (color online). The phase differences relative to the reference amplitude (2^{++} E1) for the (a) 0^{++}, (b) 2^{++} M2, and (c) 2^{++} E3 amplitudes as a function of $M_{\pi^0\pi^0}$ for the nominal results. The solid black markers show the phase differences calculated from one set of solutions, while the open red markers represent the ambiguous partner solutions. An arbitrary phase convention is applied here in which the phase difference between the 0^{++} and 2^{++} E1 amplitudes is required to be positive. Only statistical errors are presented.

two scalar light quark states and a scalar glueball [35,36]. A definitive statement on the number and properties of the scattering amplitude poles in this region of the spectrum requires model-dependent fits to the data. The effectiveness of any such model-dependent study could be greatly enhanced by including similar data from the decay $J/\psi \rightarrow \gamma K K$ in an attempt to isolate production features from partial widths to KK and $\pi\pi$ final states.

Additional structures are present in the 0^{++} amplitude below 0.6 GeV/c^2 and near 2.0 GeV/c^2. It seems reasonable to interpret the former as the σ [$f_0(500)$]. The latter could be attributed to the $f_0(2020)$. The presence of the four states below 2.1 GeV/c^2 would be consistent with the previous study of radiative J/ψ decays to $\pi\pi$ by BESII [20]. Finally, the results presented here also suggest two possible additional structures in the 0^{++} spectrum that were not observed in Ref. [20]. These include a structure just below 1 GeV/c^2, which may indicate an $f_0(980)$, but the enhancement in this region is quite small. There also appears to be some structure in the 0^{++} spectrum around 2.4 GeV/c^2.

In the 2^{++} amplitude, the results of this analysis indicate a dominant contribution from what appears to be the $f_2(1270)$, consistent with previous results [20]. However, the remaining structure in the 2^{++} amplitude appears significantly different from that assumed in the model used to obtain the BESII results [20]. In particular, the region between 1.5 and 2.0 GeV/c^2 was described in the BESII analysis with a relatively narrow $f_2(1810)$. One permutation of the nominal results (the red markers in Fig. 2) indicates that the structures in this region are much broader, while the other permutation (the black markers in Fig. 2) suggests that there is very little contribution from any 2^{++} states in this region.

The tensor spectrum near 2 GeV/c^2 is of interest in the search for a tensor glueball. Previous investigations of the $J/\psi \rightarrow \gamma\pi^0\pi^0$ channel reported evidence for a narrow ($\Gamma \approx 20$ MeV) tensor glueball candidate, $f_J(2230)$ [25]. While a model-dependent fit is required to place a limit on the production of such a state using these data, we note that based on the reported value of $B(J/\psi \rightarrow \gamma f_J(2230))$ [23], one would naively expect to observe a peak for the $f_J(2230)$ with an integral that is of order 4×10^5 but concentrated only in roughly two bins of $M(\pi^0\pi^0)$, corresponding to the full width of the $f_J(2230)$. Such a structure seems difficult to accommodate in the extracted 2^{++} amplitude.

F. Branching fraction

The results of the mass independent amplitude analysis allow for a measurement of the branching fraction of radiative J/ψ decays to $\pi^0\pi^0$, which is determined according to

$$\mathcal{B}(J/\psi \rightarrow \gamma\pi^0\pi^0) = \frac{N_{\gamma\pi^0\pi^0} - N_{\text{bkg}}}{\epsilon_\gamma N_{J/\psi}}, \qquad (15)$$

where $N_{\gamma\pi^0\pi^0}$ is the number of acceptance corrected events, N_{bkg} is the number of remaining background events, ϵ_γ is an efficiency correction necessary to extrapolate the $\pi^0\pi^0$ spectrum down to a radiative photon energy of zero, and $N_{J/\psi}$ is the number of J/ψ decays in the data. The number of acceptance corrected events is determined from the amplitude analysis by summing the total intensity from each $M_{\pi^0\pi^0}$ bin. The number of remaining background events is determined according to the inclusive and exclusive MC samples. The fractional background contamination in each bin i, $R_{\text{bkg},i}$, is determined before acceptance correction. The number of background events is then determined by assuming $R_{\text{bkg,i}}$ is constant after acceptance correction such that the number of background events in bin i, $N_{\text{bkg},i}$, is given by the product of $R_{\text{bkg},i}$ and the number of acceptance corrected events in the same bin, $N_{\gamma\pi^0\pi^0,i}$. Note that the backgrounds from J/ψ decays to $\gamma\eta(')$ are removed during the fitting process and are not included in this factor. The efficiency correction factor, ϵ_γ, is determined by calculating the fraction of phase space that is removed by applying the selection requirements on the energy of the radiative photon. This extrapolation increases the total number of events by 0.07%. Therefore, ϵ_γ is taken to be 0.9993.

The backgrounds remaining after event selection fall into three categories. The misreconstructed backgrounds are determined from an exclusive MC sample that resembles the data. Events that remain in a continuum data sample taken at 3.080 GeV after selection criteria have been applied are also taken as a background. Finally, the other remaining backgrounds are determined using the inclusive MC sample. Each of these backgrounds is scaled appropriately. In total, the acceptance corrected number of background events, N_{bkg}, is determined to be 35,951. The number of radiative J/ψ decays to $\pi^0\pi^0$, $N_{\gamma\pi^0\pi^0}$, is determined to be 1,543,050 events. The branching fraction for this decay is then determined to be $(1.151 \pm 0.002) \times 10^{-3}$, where the error is statistical only.

V. SYSTEMATIC UNCERTAINTIES

The systematic uncertainties for the mass independent analysis include two types. First, the uncertainty due to the effect of backgrounds from J/ψ decays to $\gamma\eta(')$ are addressed by repeating the analysis and treating the background in a different manner. The second type of systematic uncertainty is that due to the overall normalization of the results. Sources of systematic uncertainties of this type include the photon detection efficiency, the total number of J/ψ decays, the effect of various backgrounds, differences in the effect of the kinematic fit between the data and MC samples and the effect of model dependencies. The uncertainty on the branching fraction of π^0 to $\gamma\gamma$ according to the PDG is 0.03% [1], which is negligible in relation to the other sources of uncertainty. The systematic

TABLE II. Summary of the systematic uncertainties (in %) for the branching fraction of radiative J/ψ decays to $\pi^0\pi^0$.

Source	$J/\psi \to \gamma\pi^0\pi^0$ (%)
Photon detection efficiency	5.0
Number of J/ψ	0.8
Inclusive MC backgrounds	1.5
Non-J/ψ backgrounds	0.8
$\omega\pi^0$ background	0.8
Kinematic fit χ^2_{6C}	0.1
Model dependent comparison	0.3
Total	5.4

uncertainties are described below and summarized in Table II. These uncertainties also apply to the branching fraction measurement. Finally, several cross-checks are also performed.

A. $J/\psi \to \gamma\eta$ and $J/\psi \to \gamma\eta'$ background uncertainty

The amplitude analysis is performed with the assumption that all backgrounds have been eliminated. Studies using Monte Carlo simulation indicate this is a valid assumption for

most of the $M_{\pi^0\pi^0}$ spectrum. However, significant backgrounds from J/ψ decays to $\gamma\eta$ and $\gamma\eta'$ exist in many mass bins below about 1 GeV/c^2. Rather than inflating the errors of these bins according to the uncertainty introduced by these backgrounds, which would not take into account the bin-to-bin correlations, a set of alternate results is presented in which the $\gamma\eta(')$ backgrounds are not subtracted.

The fraction of events in J/ψ decays to $\gamma\eta(')$ that survive the event selection criteria for the $\gamma\pi^0\pi^0$ final state is very small (about 0.02%). Minor changes to the modeling of these decays may therefore have a large effect on the backgrounds. The difference between the nominal results and the alternate results, which treat the backgrounds differently, can be viewed as an estimator of the systematic error in the results due to these backgrounds.

The distinctive feature of the alternate results is an enhancement in the 0^{++} intensity in the region below about 0.6 GeV/c^2 and near the η' peak. This may be interpreted as the contribution of the events from J/ψ decays to $\gamma\eta(')$, which are being treated as signal events. A comparison of the 0^{++} amplitude for nominal results and the alternate results is presented in Fig. 4. The results for the
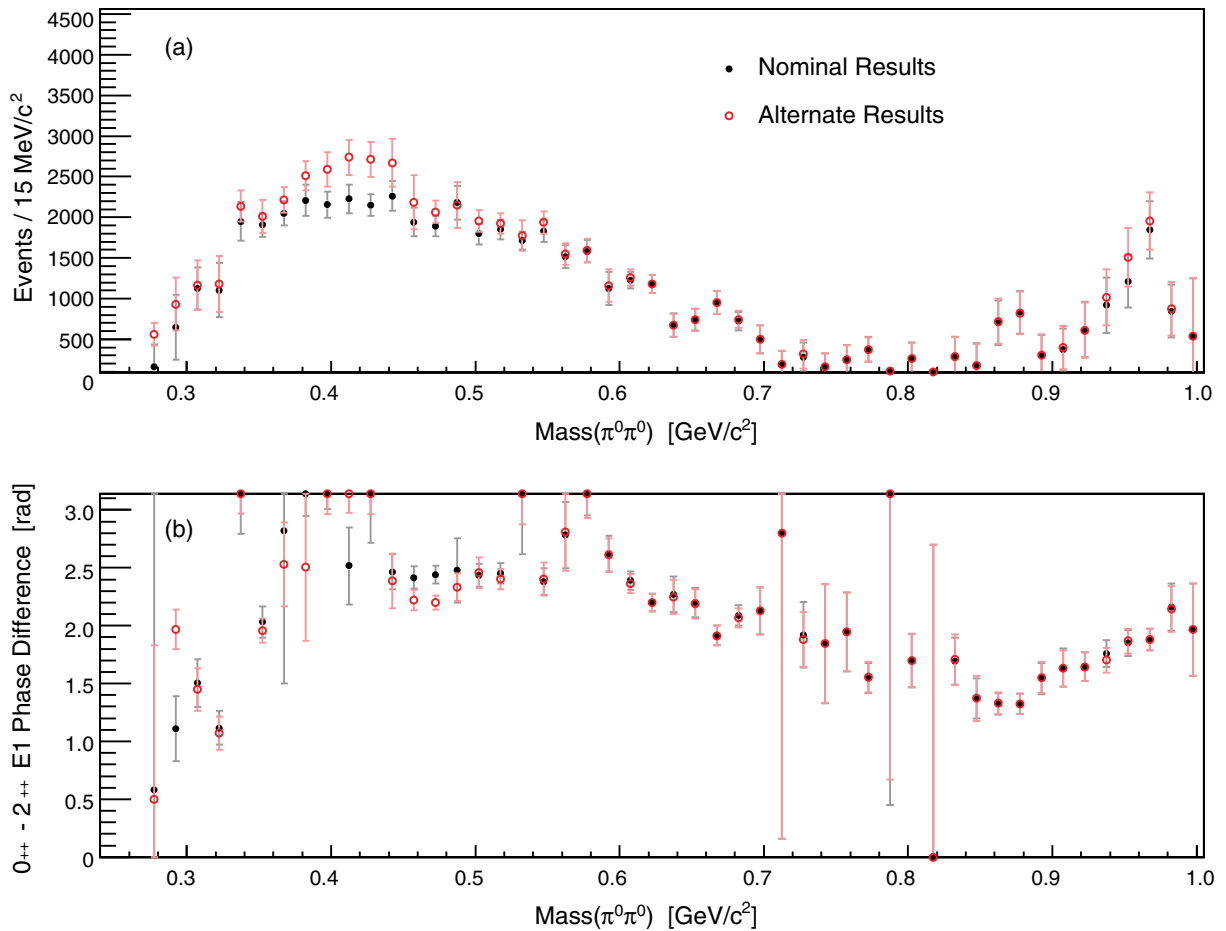

FIG. 4 (color online). A comparison of the (a) 0^{++} intensity and (b) phase difference relative to the 2^{++} E1 amplitude for the nominal results and the alternate results, in which the $\gamma\eta(')$ backgrounds have not been subtracted from the data. The solid black markers show the nominal results, while the red markers represent the alternate results. Only statistical errors are presented.

other amplitudes are consistent between the two methods. Any conclusion drawn from these data that is sensitive to choosing specifically the alternate or nominal results is not a robust conclusion.

B. Uncertainties in the overall normalization

1. Photon detection efficiency

The primary source of systematic uncertainty for this analysis comes from the reconstruction of photons. To account for this uncertainty, the photon detection efficiency of the BESIII detector is studied using the so-called tag and probe method on a sample of J/ψ decays to $\pi^+\pi^-\pi^0$, where the π^0 decays into two photons. One of these final state photons is reconstructed, along with the two charged tracks, while the other photon is left as a missing particle in the event. This information can then be used to determine the region in the detector where the missing photon is expected. The photon detection efficiency is calculated by taking the ratio of the number of missing photons that are detected in this region to the number that are expected. The numbers of detected and expected photons are determined with fits to the two photon invariant mass distributions.

The systematic uncertainty due to photon reconstruction is determined by investigating the differences between the photon detection efficiencies of the inclusive MC sample and that of the data sample. This difference is measured to be less than 1.0%, which is taken to be the systematic uncertainty per photon. For the five photon final state the overall uncertainty due to this effect is therefore taken to be 5.0%.

An additional source of uncertainty, which is due to mismodeling of the photon detection efficiency as a function of the angular and energy dependence of the radiative photon, was studied using the same channel. The phase space MC samples used for normalization in each bin of the mass independent amplitude analysis were modified to account for differences in the photon detection efficiency between the data and inclusive MC samples. The mass independent analysis was then repeated using the modified phase space MC samples. Neither the differences in angular nor energy dependence had a significant effect on the results of the analysis. The effects of mismodeling of this type are therefore taken to be negligible.

2. Number of J/ψ

The number of J/ψ decays is determined from an analysis of inclusive hadronic events

$$N_{J/\psi} = \frac{N_{\text{sel}} - N_{\text{bg}}}{\epsilon_{\text{trig}} \times \epsilon_{\text{data}}^{\psi(2S)} \times f_{\text{cor}}}, \qquad (16)$$

where N_{sel} represents the number of inclusive events remaining after selection criteria have been applied and N_{bg} is the number of background events estimated with a

data sample collected at 3.080 GeV. The efficiency for the trigger is given by ϵ_{trig}, while $\epsilon_{\text{data}}^{\psi(2S)}$ is the detection efficiency for J/ψ inclusive decays determined from $\psi(2S)$ decays to $\pi^+\pi^-J/\psi$. Finally, f_{cor} represents a correction factor to translate $\epsilon_{\text{data}}^{\psi(2S)}$ to the efficiency for inclusive decays in which the J/ψ is produced at rest. To obtain N_{sel}, at least two charged tracks are required for each event. Additionally, the momenta of these tracks and the visible energy of each event are restricted in order to eliminate Bhabha and di-muon events as well as beam gas interactions and virtual photon-photon collisions. The total number of J/ψ decays in the data sample according to Eq. (16) is determined to be $(1.311 \pm 0.011) \times 10^9$ events, which results in an uncertainty of 0.8% [26,27].

3. Background size

According to the inclusive MC sample, the total number of background events that contaminate the signal is about 1.5%. These do not include the misreconstructed backgrounds nor the backgrounds from J/ψ decays to $\gamma\eta(')$, both of which are addressed in a separate systematic uncertainty. Additionally, backgrounds from non-J/ψ decays yield a contamination of approximately 0.8%. Conservative systematic uncertainties equal to 100% of the background contamination are attributed to each of the inclusive MC and continuum background types.

4. Uncertainty in the acceptance corrected signal yield

One of the largest remaining backgrounds after signal isolation and background subtraction is the signal mimicking decay of J/ψ to $\omega\pi^0$, where the ω decays to $\gamma\pi^0$. The nominal method to address this background is to restrict the $\gamma\pi^0$ invariant mass to exclude the region within 50 MeV/c^2 of the ω mass. An alternative method is to include an amplitude for the $\omega\pi^0$ final state in the analysis. The results of this alternative method are quantitatively no different than the nominal results, suggesting that the exclusion method is an effective means of addressing the background from J/ψ decays to $\omega\pi^0$. The difference in the branching fraction using the signal yield for the alternative method compared to the nominal method is about 0.8%.

As discussed above, backgrounds due to J/ψ decays to $\gamma\eta(')$ are addressed in the fitting procedure itself by adding an exclusive MC sample to the data, but with a negative weight. The systematic uncertainty due to this background is determined by using the data alone. In this way, contributions from these backgrounds are treated as the signal and inflate the signal yield and background size in Eq. (15). The difference in the branching fraction is 0.03%, which is considered a negligible contribution to the systematic uncertainty.

Differences in the effect of the 6C kinematic fit on the data and MC samples may cause a systematic difference in the acceptance corrected signal yield. This effect was

investigated by loosening the restriction on the χ^2 from the 6C kinematic fit. For events with a $M_{\pi^0\pi^0}$ above the KK threshold, this restriction was relaxed from less than 60 to be less than 125. Events with an invariant mass below the KK threshold are required to have a χ^2 less than 60 rather than less than 20. The difference in the branching fraction for the results with the loosened χ^2 cut relative to that of the nominal results is about 0.1%.

Another source of systematic uncertainty in the branching fraction is the difference between the nominal results and those obtained by applying a model that describes the $\pi\pi$ dynamics. To test this effect, a mass dependent fit using interfering Breit-Wigner line shapes was performed. The difference in the branching fraction using the acceptance corrected yield of the mass dependent analysis compared to the nominal results is about 0.3%.

The effect of the remaining misreconstructed backgrounds on the results is studied by performing a closure test, in which the mass independent amplitude analysis is performed on an exclusive MC sample. This MC sample was generated according to the results of a mass dependent amplitude analysis of the data and includes the proper angular distributions. After applying the same selection criteria that are applied to the data, the MC sample is passed through the mass independent analysis. This process is repeated after removing the remaining misreconstructed backgrounds from the sample. The difference in the branching fraction between these two methods is 0.01%. The effect of these backgrounds is therefore taken to be negligible.

C. 4^{++} amplitude

As discussed above, the only $\pi^0\pi^0$ amplitudes that are accessible in radiative J/ψ decays have even angular momentum and positive parity and charge conjugation quantum numbers. The mass independent analysis was performed under the assumption that only the 0^{++} and 2^{++} amplitudes are significant. To test this assumption, the analysis was repeated with the addition of a 4^{++} amplitude. No significant contribution from a 4^{++} amplitude is apparent.

To test the effect of a 4^{++} amplitude that may exist in the data and is ignored in the fit, an exclusive MC sample was generated using a model constructed from a sum of resonances each parametrized by a Breit-Wigner function in a way that optimally reproduces the data. One of the resonances was an $f_4(2050)$, which was generated in each component of the 4^{++} amplitude. The relative size of the 4^{++} amplitude was determined from a mass dependent fit to the data, in which the 4^{++} amplitude contributed 0.43% to the overall intensity. A mass independent amplitude analysis, which did not include a 4^{++} amplitude, was then performed on this sample. The results indicate that the intensities and phases for the 0^{++} and 2^{++} amplitudes deviate from the input parameters at the order of the statistical errors from the data sample in the region between 1.5 and 3.0 GeV/c^2. Therefore, the systematic error due to

the effect of ignoring a possible 4^{++} amplitude is estimated to be of the same order as the statistical errors in the region from 1.5 to 3.0 GeV/c^2.

VI. CONCLUSIONS

A mass independent amplitude analysis of the $\pi^0\pi^0$ system in radiative J/ψ decays is presented. This analysis uses the world's largest data sample of its type, collected with the BESIII detector, to extract a piecewise function that describes the scalar and tensor $\pi\pi$ amplitudes in this decay. While the analysis strategy employed to obtain results has complications, namely ambiguous solutions, a large number of parameters, and potential bias in subsequent analyses from non-Gaussian effects (see Appendix C), it minimizes systematic bias arising from assumptions about $\pi\pi$ dynamics and, consequently, permits the development of dynamical models or parametrizations for the data.

In order to facilitate the development of models, the results of the mass independent analysis are presented in two ways. The intensities and phase differences for the amplitudes in the fit are presented here as a function of $M_{\pi^0\pi^0}$. Additionally, the intensities and phases for each bin of $M_{\pi^0\pi^0}$ are given in supplemental materials (see Appendix C). These results may be combined with those of similar reactions for a more comprehensive study of the light scalar meson spectrum. Finally, the branching fraction of radiative J/ψ decays to $\pi^0\pi^0$ is measured to be $(1.15 \pm 0.05) \times 10^{-3}$, where the error is systematic only and the statistical error is negligible. This is the first measurement of this branching fraction.

APPENDIX A: AMPLITUDES

The amplitude for radiative J/ψ decays to $\pi^0\pi^0$ can be determined in different bases depending on the information of interest. For example, in the helicity basis, the amplitude depends on the angular momentum and helicity of the $\pi^0\pi^0$ resonance as well as the angular momentum and polarization of the J/ψ. It is also possible to relate the amplitudes to radiative multipole transitions. Such a basis is useful because it may allow implementation or testing of dynamical assumptions. For example, a model may suggest that the E1 radiative transition should dominate over the M2 transition.

In the radiative multipole basis, the amplitude for radiative J/ψ decays to $\pi^0\pi^0$ is given by

$$U^{M,\lambda_\gamma}(\vec{x},s) = \sum_{j,J_\gamma,\mu} N_{J_\gamma} N_j D^J_{M,\mu-\lambda_\gamma}(\pi+\phi_\gamma,\pi-\theta_\gamma,0)$$

$$\times D^j_{\mu,0}(\phi_\pi,\theta_\pi,0)\frac{1}{2}\frac{1+(-1)^j}{2}$$

$$\times \langle J_\gamma-\lambda_\gamma;j\mu|J\mu-\lambda_\gamma\rangle$$

$$\times \frac{1}{\sqrt{2}}[\delta_{\lambda_\gamma,1}+\delta_{\lambda_\gamma,-1}P(-1)^{J_\gamma-1}]V_{j,J_\gamma}(s), \quad \text{(A1)}$$

where the parity, total angular momentum, and helicity of the pair of pseudoscalars are given by P, j, and μ, respectively. The D functions are the familiar Wigner D-matrix elements. The angular momentum of the photon, J_γ, is related to the nuclear radiative (E1, M2, E3, etc.) transitions. Each amplitude is characterized by the angular momentum of the photon and the angular momentum of the pseudoscalar pair. The possible values of J_γ are limited by the conservation of angular momentum. The helicity of the radiative photon is given by λ_γ. The total angular momentum and polarization of the J/ψ are given by J and M, respectively. Finally, $N_j = \sqrt{\frac{2j+1}{4\pi}}$ is a normalization factor.

The angles $(\phi_\gamma,\theta_\gamma)$ are the azimuthal and polar angles of the photon in the rest frame of the J/ψ, where the direction of

the J/ψ momentum defines the x axis. The angles (ϕ_π,θ_π) are the azimuthal and polar angles of one π^0 in the rest frame of the $\pi^0\pi^0$ pair, with the z axis along the direction of the photon momentum and the x axis defined by the direction perpendicular to the plane shared by the beam and the z axis.

Parity is a conserved quantity for strong and electromagnetic interactions. Hence, for J/ψ radiative decays, $P=(-1)^j$ must be positive. This means that the only intermediate states available have $j^P=0^+,2^+,4^+$, etc. Additionally, isospin conservation in strong interactions requires I^G for the intermediate state to be 0^+ (isoscalar). The complex function $V_{j,J_\gamma}(s)$ describes the $\pi^0\pi^0$ production and decay dynamics. In order to minimize the model dependence of the mass independent analysis, the dynamical amplitude is replaced by a (complex) free parameter in the unbinned extended maximum likelihood fit. Thus, the amplitude, in a region around s is given by

$$U^{M,\lambda_\gamma}(\vec{x},s) = \sum_{j,J_\gamma} V_{j,J_\gamma} A^{M,\lambda_\gamma}_{j,J_\gamma}(\vec{x}), \quad \text{(A2)}$$

where

$$A^{M,\lambda_\gamma}_{j,J_\gamma}(\vec{x}) = N_{J_\gamma} N_j D^J_{M,\mu-\lambda_\gamma}(\pi+\phi_\gamma,\pi-\theta_\gamma,0)$$

$$\times D^j_{\mu,0}(\phi_\pi,\theta_\pi,0)\frac{1}{2}\frac{1+(-1)^j}{2}$$

$$\times \langle J_\gamma-\lambda_\gamma;j\mu|J\mu-\lambda_\gamma\rangle$$

$$\times \frac{1}{\sqrt{2}}[\delta_{\lambda_\gamma,1}+\delta_{\lambda_\gamma,-1}P(-1)^{J_\gamma-1}], \quad \text{(A3)}$$

and $\{j,J_\gamma\}$ represents the unique amplitudes accessible for the given set of observables, $\{M,\lambda_\gamma\}$.

APPENDIX B: AMBIGUITIES

One of the challenges of amplitude analysis is the issue of ambiguous solutions, two solutions that give the same distribution (e.g., Ref. [7]). In this section, the ambiguous solutions for radiative J/ψ decays to $\pi^0\pi^0$ are studied.

To determine the angular dependence of the amplitudes, it is necessary to write the decay amplitude $A^{M,\lambda_\gamma}_{j,J_\gamma}(\vec{x})$, which is given in Eq. (A1), explicitly as a function of the angles $(\phi_\gamma,\theta_\gamma)$ and (ϕ_π,θ_π). The Clebsch-Gordan factors in the amplitude restrict the signs of μ to be the same as that of λ_γ. Thus, for $j=2$ and $\lambda_\gamma=1$, only the values $\mu=0,1,2$ give nonzero amplitude contributions. It is also important to note that the Clebsch-Gordan coefficients will change sign under $\lambda_\gamma\to-\lambda_\gamma$, but only for $J_\gamma=2$. This will cancel the delta functions in the decay amplitude with the result

$$A^{M,\lambda_\gamma}_{j,J_\gamma}(\vec{x}) = \sum_\mu c^{J_\gamma,\lambda_\gamma}_{j,\mu} N_{J_\gamma} N_j e^{-iM(\pi+\phi_\gamma)} d^1_{M,\mu-\lambda_\gamma}(\pi-\theta_\gamma) \times e^{-i\mu\phi_\pi} d^j_{\mu,0}(\theta_\pi)\frac{1}{\sqrt{2}}[\delta_{\lambda_\gamma,1}+\delta_{\lambda_\gamma,-1}(-1)^{J_\gamma-1}], \quad \text{(B1)}$$

where the constants $c_{j,\mu}^{J_\gamma,\lambda_\gamma}$ contain the Clebsch-Gordan coefficients.

Recall that, for the Wigner small d-matrix elements, $d_{1,\pm1}^1(\pi - \theta) = d_{1,\mp1}^1(\theta)$ and $d_{1,0}^1(\pi - \theta) = d_{1,0}^1(\theta)$. Then, $d_{M,\mu-\lambda_\gamma}^1(\pi - \theta) = d_{M,\lambda_\gamma-\mu}^1(\theta)$. Also, note that the restrictions on μ mean that the quantity $\mu - \lambda_\gamma = \pm1, 0$. It is also useful to note that $\mu - \lambda_\gamma = \lambda_\gamma, 0, -\lambda_\gamma$, for $\mu = \pm2, \pm1, 0$, respectively. The usefulness of these features appears when one writes out the intensity for a given choice of M and λ_γ. It is also useful to plug in the values for the constants, which are given in Table III. The intensity in bin α for a given choice of observables is then given by

$$I_\alpha(\vec{x}) = \sum_{M,\lambda_\gamma} |h_0(\theta_\pi)d_{M,\lambda_\gamma}^1(\theta_\gamma)e^{i\lambda_\gamma\phi_\pi} + h_1(\theta_\pi)d_{M,0}^1(\theta_\gamma)$$
$$+ h_2(\theta_\pi)d_{M,-\lambda_\gamma}^1(\theta_\gamma)e^{-i\lambda_\gamma\phi_\pi}|^2, \quad \text{(B2)}$$

where terms with the same angular dependencies have been grouped according to

$$h_0(\theta_\pi) = \sqrt{3}V_{0,1} + \sqrt{\frac{3}{2}}(V_{2,1} + \sqrt{5}V_{2,2} + 2V_{2,3})d_{0,0}^2(\theta_\pi),$$

$$h_1(\theta_\pi) = \frac{1}{\sqrt{2}}(3V_{2,1} + \sqrt{5}V_{2,2} - 4V_{2,3})d_{1,0}^2(\theta_\pi),$$

$$h_2(\theta_\pi) = (3V_{2,1} - \sqrt{5}V_{2,2} + V_{2,3})d_{2,0}^2(\theta_\pi), \quad \text{(B3)}$$

and the subscripts on the production amplitudes represent the possible combinations of j and J_γ. The following calculations apply for each bin individually.

The amplitudes for which M and λ_γ have the same (opposite) sign, $M = \lambda_\gamma = \pm1$ ($M = -\lambda_\gamma = \pm1$), are related to each other by a sign change in the exponential factor. Note that the terms with a factor of $d_{M,0}^1$ will change sign under $M \to -M$ and terms with a factor of $d_{\mu,0}^j$ will change sign under $\lambda_\gamma \to -\lambda_\gamma$. Then, the intensity becomes

$$I(\vec{x}) = \sum_{M=\lambda_\gamma=\pm1} |h_0(\theta_\pi)d_{1,1}^1(\theta_\gamma)e^{\pm i\phi_\pi} + h_1(\theta_\pi)d_{1,0}^1(\theta_\gamma)$$
$$+ h_2(\theta_\pi)d_{1,-1}^1(\theta_\gamma)e^{\mp i\phi_\pi}|^2$$
$$+ \sum_{M=-\lambda_\gamma=\pm1} |h_0(\theta_\pi)d_{1,-1}^1(\theta_\gamma)e^{\pm i\phi_\pi} - h_1(\theta_\pi)d_{1,0}^1(\theta_\gamma)$$
$$+ h_2(\theta_\pi)d_{1,1}^1(\theta_\gamma)e^{\mp i\phi_\pi}|^2. \quad \text{(B4)}$$

TABLE III. The constant factors in Eq. (B1) are given here.

$c_{0,0}^{J_\gamma,\lambda_\gamma} = 1$		
$c_{2,0}^{1,\pm1} = \sqrt{\frac{1}{10}}$	$c_{2,0}^{2,\pm1} = \pm\sqrt{\frac{3}{10}}$	$c_{2,0}^{3,\pm1} = \sqrt{\frac{6}{35}}$
$c_{2,1}^{1,\pm1} = \sqrt{\frac{3}{10}}$	$c_{2,1}^{2,\pm1} = \pm\sqrt{\frac{1}{10}}$	$c_{2,1}^{3,\pm1} = -\sqrt{\frac{8}{35}}$
$c_{2,2}^{1,\pm1} = \sqrt{\frac{3}{5}}$	$c_{2,2}^{2,\pm1} = \mp\sqrt{\frac{1}{5}}$	$c_{2,2}^{3,\pm1} = \sqrt{\frac{1}{35}}$

Note that the term with $h_1(\theta_\pi)$ has changed sign in the opposite combination. The properties of small d functions, $d_{m',m}^j(\theta) = (-1)^{m-m'}d_{m,m'}^j(\theta) = d_{-m,-m'}^j(\theta)$, have been used to write the incoherent pieces of the intensity in the same way.

It is instructive to write the intensity function as

$$I(\vec{x}) = f_0 + f_1 \cos 2\theta_\gamma + \frac{1}{2}f_2 \cos 2\phi_\pi$$
$$+ \frac{1}{2}f_3 \sin 2\theta_\gamma \cos\phi_\pi - \frac{1}{2}f_4 \cos 2\theta_\gamma \cos 2\phi_\pi, \quad \text{(B5)}$$

where

$$f_0 = \frac{3}{2}[(h_0)^2 + (h_2)^2] + (h_1^2),$$

$$f_1 = \frac{1}{2}[(h_0)^2 + (h_2)^2] - (h_1)^2,$$

$$f_2 = f_4 = (h_0 h_2^* + h_0^* h_2),$$

$$f_3 = \sqrt{2}(-h_0 h_1^* - h_0^* h_1 + h_2 h_1^* + h_2^* h_1). \quad \text{(B6)}$$

Now, if a set of amplitude couplings, V, have been determined by fitting the intensity function in Eq. (B5) to the data, ambiguities would arise if an alternative set of couplings, V', would give the same angular dependence as the original set. In other words, the new set of amplitudes must give the same values for the f_i functions ($f_i' = f_i$).

Consider f_2, which can be written as a linear combination of two quadratic forms

$$f_2 = \frac{1}{2}(|h_0 + h_2|^2 - |h_0 - h_2|^2). \quad \text{(B7)}$$

These quadratic forms are given by

$$|h_0 \pm h_2|^2 = [\cos^2\theta_\pi(3a_1 \mp a_3) + (b - a_1 \pm a_3)]$$
$$\times [\cos^2\theta_\pi(3a_1^* \mp a_3^*) + (b^* - a_1^* \pm a_3^*)], \quad \text{(B8)}$$

where for simplicity the production coefficients have been combined into new variables given by

$$b = \sqrt{3}V_{0,1},$$

$$a_1 = \frac{\sqrt{6}}{4}(V_{2,1} + \sqrt{5}V_{2,2} + 2V_{2,3}),$$

$$a_2 = -\frac{\sqrt{3}}{4}(3V_{2,1} + \sqrt{5}V_{2,2} - 4V_{2,3}),$$

$$a_3 = \frac{\sqrt{6}}{4}(3V_{2,1} - \sqrt{5}V_{2,2} + V_{2,3}). \quad \text{(B9)}$$

Since only the absolute square of each combination of h_0 and h_2 appears in the intensity, nontrivial ambiguous solutions appear only when the production coefficients are replaced by their complex conjugate for one choice of sign in Eq. (B8). That is, if $u_1 = (b, a_1, a_2, a_3)$ and $u_2 = (b', a_1', a_2', a_3')$, the solutions $\{u_1, u_2\}$ and $\{u_1, u_2^*\}$ should give consistent values for $h_0 \pm h_2$. This requires that either

$$h'_0 + h'_2 = h^*_0 + h^*_2,$$
$$h'_0 - h'_2 = h_0 - h_2 \qquad (B10)$$

or

$$h'_0 + h'_2 = h_0 + h_2,$$
$$h'_0 - h'_2 = h^*_0 - h^*_2. \qquad (B11)$$

Therefore, either

$$3a'_1 - a'_3 = 3a^*_1 - a^*_3,$$
$$b' - a'_1 + a'_3 = b^* - a^*_1 + a^*_3,$$
$$3a'_1 + a'_3 = 3a_1 + a_3,$$
$$b' - a'_1 - a'_3 = b - a_1 - a_3 \qquad (B12)$$

or

$$3a'_1 - a'_3 = 3a_1 - a_3,$$
$$b' - a_1' + a'_3 = b - a_1 + a_3,$$
$$3a'_1 + a'_3 = 3a^*_1 + a^*_3,$$
$$b' - a'_1 - a'_3 = b^* - a^*_1 - a^*_3. \qquad (B13)$$

Both Eq. (B12) and Eq. (B13) require that

$$\mathrm{Im}\, b = -2\,\mathrm{Im}\, a_1. \qquad (B14)$$

The difference between Eq. (B12) and Eq. (B13) is a sign change for the imaginary part of each amplitude. This difference is equivalent to the trivial ambiguities discussed in Sec. IV D. Let us choose the phase convention given by Eq. (B12). Finally, the invariance of f_1, given the conditions above, requires that $a'_2 = a_2$.

Using the conditions in Eq. (B12) and the constraint $a'_2 = a_2$, the alternate set of solutions can be written in terms of the original set as

$$\mathrm{Re} V'_{0,1} = \mathrm{Re} V_{0,1},$$

$$\mathrm{Im} V'_{0,1} = -\frac{1}{3\sqrt{2}}(3\mathrm{Im} V_{2,1} - \sqrt{5}\mathrm{Im} V_{2,2} + \mathrm{Im} V_{2,3}),$$

$$\mathrm{Re} V'_{2,1} = \mathrm{Re} V_{2,1},$$

$$\mathrm{Im} V'_{2,1} = \mathrm{Im} V_{2,1} + \frac{2\sqrt{5}}{3}\mathrm{Im} V_{2,2} + \frac{5}{6}\mathrm{Im} V_{2,3},$$

$$\mathrm{Re} V'_{2,2} = \mathrm{Re} V_{2,2},$$

$$\mathrm{Im} V'_{2,2} = -\mathrm{Im} V_{2,2} - \frac{\sqrt{5}}{2}\mathrm{Im} V_{2,3},$$

$$\mathrm{Re} V'_{2,3} = \mathrm{Re} V_{2,3},$$

$$\mathrm{Im} V'_{2,3} = \mathrm{Im} V_{2,3}. \qquad (B15)$$

Note that the last two lines of Eq. (B15) indicate that the ambiguous solution for the 2^{++} E3 amplitude is redundant with the original solution. That is, the 2^{++} E3 amplitude does not exhibit multiple solutions.

In a practical sense, these results are useful to compare the mathematical predictions to what is found experimentally. Essentially, the predicted ambiguous partner for a set of fit results in a given bin may be calculated in the following way. First, the results must be rotated in phase space such that the condition in Eq. (B14) is satisfied. Next, the ambiguous partner may be determined using Eq. (B15). Finally, this predicted solution must be rotated back into the original phase convention. Now, the predicted ambiguous partner may be compared with the experimentally determined fit results. Studies show that the mathematically predicted ambiguities match those found experimentally.

APPENDIX C: SUPPLEMENTAL MATERIALS

In addition to the figures presented here, the results of the mass independent analysis in each bin of $M_{\pi^0\pi^0}$ are included in the supplemental materials [37]. This includes the intensities of each amplitude and the three phase differences for each bin of $M_{\pi^0\pi^0}$. The two ambiguous solutions of the nominal results are separated into two text files, while one additional text file contains the alternate results in the region where they are not redundant with the nominal results. Note that these results contain only statistical errors.

It is important to reiterate that errors reported in the supplemental results (and in the figures in the text) are derived from the covariance matrix of the fit parameters. That is, they are valid in the Gaussian limit, a limit that cannot be guaranteed for all parameters in the analysis. Therefore the use of these results in a subsequent fit to parameters of interest cannot be expected to produce statistically rigorous values of the parameters. Likewise a χ^2 or likelihood-ratio test of a model describing the results cannot be rigorously constructed.

An attempt to quantify the potential systematic bias in subsequent analyses was made as follows. First, a MC sample with equivalent statistical precision to the data was generated using a model consisting of a coherent sum of Breit-Wigner resonances in a way that best approximates the data. A mass independent amplitude analysis was performed on this MC sample using the same procedure that was applied to the actual data reported in this analysis. The results of this mass independent analysis of the MC sample were then fit with a Breit-Wigner model, the same model with which they were generated, where the couplings of the Breit-Wigner distributions in the model were allowed to float as free parameters. While most fit parameters exhibited typical Gaussian fluctuations about their known input values, there were some non-Gaussian outliers. About one-third of the parameters exhibited deviations from input at or above the three sigma level. In

comparison with a mass dependent analysis, in which the Breit-Wigner model is directly fit to the same mock data, the parameter errors in the model fit to the mass independent results were generally larger, typically within a factor of 2, but in some cases by up to a factor of 10.

To probe the scale of the systematic deviations of the fitted values from the true input values used to generate our MC sample, for each amplitude we used the true value of the coupling instead of the fitted value and computed (1) the total intensity integrated over all phase space and

(2) the fit fraction (ratio of individual amplitude intensity to total intensity). We observe the deviations in (1) to be at or below the 1% level for all amplitudes and the deviations in (2) to be at or below 2% on an absolute scale for all amplitudes. For small amplitudes, this means that relative deviations in intensity may occur at a level of 10%-90%. This suggests validity and precision at a level sufficient for model development; however, rigorous values for any model parameters can only be reliably obtained by fitting the given model directly to the data.

[1] J. Beringer *et al.* (Particle Data Group), Phys. Rev. D **86**, 010001 (2012).

[2] G. S. Bali, K. Shilling, A. Hulsebos, A. C. Irving, C. Michael, and P. Stephenson, Phys. Lett. B **309**, 378 (1993).

[3] C. J. Morningstar and M. J. Peardon, Phys. Rev. D **60**, 034509 (1999).

[4] Y. Chen, A. Alexandru, S. J. Dong, T. Draper, I. Horvath, F. X. Lee, K. F. Liu, N. Mathur, C. Morningstar, M. Peardon, S. Tamhankar, B. L. Young, and J. B. Zhang, Phys. Rev. D **73**, 014516 (2006).

[5] W. Ochs, J. Phys. G **40**, 043001 (2013).

[6] J. R. Pelaez and F. J. Yndurain, Phys. Rev. D **71**, 074016 (2005).

[7] J. Gunter *et al.* (E852 Collaboration), Phys. Rev. D **64**, 072003 (2001).

[8] A. Abele *et al.* (Crystal Barrel Collaboration), Phys. Lett. B **380**, 453 (1996).

[9] R. Bellazzini *et al.* (GAMS Collaboration), Phys. Lett. B **467**, 296 (1999).

[10] M. Ablikim *et al.* (BES Collaboration), Phys. Lett. B **645**, 19 (2007).

[11] M. Ablikim *et al.* (BES Collaboration), Phys. Lett. B **607**, 243 (2005).

[12] M. Ablikim *et al.* (BES Collaboration), Phys. Lett. B **598**, 149 (2004).

[13] M. Ablikim *et al.* (BES Collaboration), Phys. Lett. B **603**, 138 (2004).

[14] J. P. Lees *et al.* (*BABAR* Collaboration), Phys. Rev. D **85**, 112010 (2012).

[15] G. Bonvicini *et al.* (CLEO Collaboration), Phys. Rev. D **76**, 012001 (2007).

[16] J. R. Batley *et al.* (NA48/2 Collaboration), Eur. Phys. J. C **54**, 411 (2008).

[17] T. Mori *et al.* (Belle Collaboration), Phys. Rev. D **75**, 051101 (2007).

[18] A. Aloisio *et al.* (KLOE Collaboration), Phys. Lett. B **537**, 21 (2002).

[19] V. Anisovich and A. Sarantsev, Eur. Phys. J. A **16**, 229 (2003).

[20] M. Ablikim *et al.* (BES Collaboration), Phys. Lett. B **642**, 441 (2006).

[21] R. M. Baltrusaitis *et al.* (Mark-III Collaboration), Phys. Rev. D **35**, 2077 (1987).

[22] J. E. Augustin *et al.* (DM2 Collaboration), Z. Phys. C **36**, 369 (1987).

[23] J. Z. Bai *et al.* (BES Collaboration), Phys. Rev. Lett. **76**, 3502 (1996).

[24] L. Kopke and N. Wermes, Phys. Rep. **174**, 67 (1989).

[25] J. Z. Bai *et al.* (BES Collaboration), Phys. Rev. Lett. **81**, 3091 (1998).

[26] M. Ablikim *et al.* (BES Collaboration), Chin. Phys. C **36**, 915 (2012).

[27] M. Ablikim *et al.* (BES Collaboration). The total number of J/ψ events taken in 2009 and 2012 is determined to be 1310.6×10^6 with an uncertainty 0.8% with the same approach as that used in Ref. [26]. (2014).

[28] M. Ablikim *et al.* (BES Collaboration), Nucl. Instrum. Methods Phys. Res., Sect. A **614**, 345 (2010).

[29] Z. Y. Deng, G. F. Cao, C. D. Fu, M. He, H. M. Liu, Y. J. Mao, Y. Xia, Z. Y. You, Y. Yuan, R. Tang, Y.-J. Liu, Q.-M. Ma, and X. Ma, Chin. Phys. C **30**, 371 (2006).

[30] S. Jadach, B. F. L. Ward, and Z. Was, Comput. Phys. Commun. **130**, 260 (2000).

[31] D. J. Lange, Nucl. Instrum. Methods Phys. Res., Sect. A **462**, 152 (2001).

[32] J. C. Chen, G. S. Huang, X. R. Qi, D. H. Zhang, and Y. S. Zhu, Phys. Rev. D **62**, 034003 (2000).

[33] T. Kunihiro, Prog. Theor. Phys. Suppl. **149**, 56 (2003).

[34] C. Amsler and N. A. Tornqvist, Phys. Rep. **389**, 61 (2004).

[35] F. E. Close and A. Kirk, Eur. Phys. J. C **21**, 531 (2001).

[36] L. S. Celenza, S. F. Gao, B. Huang, H. Wang, and C. M. Shakin, Phys. Rev. C **61**, 035201 (2000).

[37] See supplemental material at http://link.aps.org/supplemental/10.1103/PhysRevD.92.052003 for text files that contain the intensities of each amplitude and the three phase differences for each bin of the mass independent amplitude analysis.